

1 **Carbon emission and export from Ket River, western Siberia**

2
3 **Artem G. Lim¹, Ivan V. Krickov¹, Sergey N. Vorobyev¹,**

4 **Mikhail A. Korets², Sergey Kopysov¹,**

5 **Liudmila S. Shirokova³, Jan Karlsson⁴, and Oleg S. Pokrovsky^{5*}**

6
7 *¹BIO-GEO-CLIM Laboratory, Tomsk State University, Tomsk, Russia*

8 *²V.N. Sukachev Institute of Forest of the Siberian Branch of Russian Academy of Sciences – separated*
9 *department of the KSC SB RAS, Krasnoyarsk, 660036, Russia*

10 *³N. Laverov Federal Center for Integrated Arctic Research, Russian Academy of Sciences, Arkhangelsk,*
11 *Russia*

12 *⁴Climate Impacts Research Centre (CIRC), Department of Ecology and Environmental Science, Umeå*
13 *University, Linnaeus väg 6, 901 87 Umeå, Sweden.*

14 *⁵Geosciences and Environment Toulouse, UMR 5563 CNRS, 14 Avenue Edouard Belin 31400 Toulouse,*
15 *France*

16
17 Key words: CO₂, C, emission, boreal, river, export, landscape, Siberia

18
19 * email: oleg.pokrovsky@get.omp.eu

20

21

22

23

24

25

26

27

28

29

30

31

32

33 **Abstract**

34 Despite recent progress in the understanding of the carbon (C) cycle of Siberian permafrost-affected
35 rivers, spatial and seasonal dynamics of C export and emission from medium-size rivers (50,000 - 300,000
36 km² watershed area) remain poorly known. Here we studied one of the largest tributaries of the Ob River, the
37 Ket River (watershed = 94,000 km²) which drains through pristine taiga forest of the boreal zone in western
38 Siberian Lowland (WSL). We combined continuous and discrete measurements of carbon dioxide (CO₂)
39 concentration using submersible CO₂ sensor and floating chamber flux (FCO₂), with methane (CH₄), organic
40 and inorganic C (DOC and DIC, respectively), particulate organic C and total bacterial concentrations over a
41 800-km transect of the Ket River main stem and its 26 tributaries during spring flood (May 2019) and 12
42 tributaries during summer baseflow (end of August – beginning of September 2019). The partial pressure of
43 CO₂ (pCO₂) was lower and less variable in the main stem (2000 to 2500 μatm) compared to that in tributaries
44 (2000 to 5000 μatm). In the tributaries, the pCO₂ was 40 % higher during baseflow compared to spring flood,
45 whereas in the main stem, it did not vary significantly across the seasons. The methane concentration in the
46 main stem and tributaries was a factor of 300 to 1900 (flood period) and 100 to 150 times lower than that of
47 CO₂, and ranged from 0.05 to 2.0 μmol L⁻¹. The FCO₂ ranged from 0.4 to 2.4 g C m⁻² d⁻¹ in the main channel
48 and from 0.5 to 5.0 g C m⁻² d⁻¹ in the tributaries, being the highest during August in tributaries and weakly
49 dependent on season in the main channel. During summer baseflow, the DOM aromaticity, bacterial number,
50 and needleleaf forest coverage of the watershed positively affected CO₂ concentrations and fluxes. We
51 hypothesize that relatively low spatial and seasonal variability in FCO₂ of the Ket River is due to flat
52 homogeneous landscape (bogs and taiga forest) that results in long water residence times and stable input of
53 allochthonous DOM, which dominate the FCO₂. The open water period (May to October) C emission from
54 the fluvial network (main stem and tributaries) of the Ket River was estimated to 127±11 Gg C y⁻¹ which is
55 lower than the downstream dissolved and particulate C export during the same period. The estimated fluvial
56 C emissions are highly conservative and contain uncertainties, linked to ignoring hot spots and hot moments
57 of emissions, notably in the floodplain zone. This stresses the need of improving temporal resolution of FCO₂
58 and water coverage across seasons and emphasizes the important role of WSL rivers for release of CO₂ to the
59 atmosphere.

60 **Introduction**

61 Assessment of greenhouse gas (GHG) emission from rivers is crucially important for understanding
62 the C cycle under various climate change scenarios (Campeau and del Giorgio, 2014; Chadburn et al., 2017;
63 Tranvik et al., 2018; Vonk et al., 2019; Vachon et al., 2020). Rivers receive terrestrial C and process and emit
64 a significant share of this C during transit to the sea (Liu et al., 2022). Quantifications of riverine C emissions
65 are sufficiently robust for relatively well studied regions of the world such as the European and N American
66 boreal zone (Dawson et al., 2004; Dinsmore et al., 2013; Wallin et al., 2013; Leith et al., 2015; Zolkos et al.,
67 2019; Hutchins et al., 2020), or Arctic and subarctic rivers of Alaska (Striegl et al., 2012; Crawford et al.,
68 2013; Stackpoole et al., 2017), although subjected to great uncertainty. Despite significant progress in
69 assessing riverine pCO₂ in previously under-represented or ignored regions such as lotic systems of Asia (Ran
70 et al., 2015, 2017; Varol and Li, 2017) or South America (Almeida et al., 2017), these studies generally use
71 a combination of pH and alkalinity (DIC) to calculate the pCO₂ instead of direct in-situ measurements, alike
72 the studies of global emissions (Raymond et al., 2013; Lauerwald et al., 2015). At the same time, there is a
73 growing number of studies reporting directly measured riverine pCO₂ – either discretely (Alin et al. 2011;
74 Borges et al., 2015; Amaral et al. 2018; 2022; Leng et al. 2022), continuously at fixed sites (Crawford et al.
75 2016a, Schneider et al. 2020; Gómez-Gener et al. 2021a), or along the river flow (Abril et al. 2014; Crawford
76 et al. 2016b; 2017; Borges et al. 2019). However, these studies are limited to tropical and temperate zones of
77 the world, and boreal regions of Western Europe and Northern America, and thus, further continuous and
78 discrete measurements of CO₂ concentration and fluxes in rivers from under-represented regions such as
79 Northern Eurasia are needed.

80 Indeed, despite their currently sub-ordinary role in global riverine CO₂ emissions (30% temperate,
81 13% Arctic regions, Liu et al., 2022), high latitude regions are important because of their large C stocks,
82 partly located in the permafrost, and their extreme vulnerability to observed and projected warming, which
83 can release 80 Pg C upon abrupt thaw and up to 200 Pg C upon gradual thaw by 2300 (Turetsky et al., 2020).
84 This is especially true for Siberia, hosting large C stocks in soils and wetlands intersected by extensive river
85 networks that deliver majority of water and C to the Arctic Ocean (Feng et al., 2013). There has been
86 substantial progress in quantification of carbon export and emissions from Siberian permafrost-affected rivers

87 (Lobbes et al., 2000; Raymond et al., 2007; Cooper et al., 2008; Semiletov et al., 2011; Feng et al., 2013;
88 Griffin et al., 2018; Wild et al., 2019). However, spatial and seasonal features of C export and emission from
89 tributaries of Siberian rivers are still remain poorly known. Existing data (Denfeld et al., 2013; Serikova et
90 al., 2018; Karlsson et al., 2021; Vorobyev et al., 2021) suggest that C (predominantly as CO₂) emissions from
91 Siberian rivers can vary largely over space and time. Such high variations do not allow reliable quantitative
92 assessment of C emission and integrating these values into regional and global C models.

93 In order to better understand and constrain the magnitude of C emission from Siberian rivers, we
94 studied the Ket River (watershed 94,000 km²), a typical tributary of the Ob River in western Siberia. The Ob
95 river is the largest (in terms of watershed area) Siberian river and drains large pristine territories of taiga forest
96 and bogs. The catchment of Ob includes extensive regions of permafrost but a major part of it (80 %) is
97 situated in the permafrost-free zone of which very few data exist on riverine C emissions (Karlsson et al.,
98 2021). The Ket river drains through dense southern taiga forest and abundant wetlands with almost no human
99 activity, thus serving a representative system for understanding C cycling in permafrost-free Siberian rivers.
100 We followed, via a boat routing over the main stem and main tributaries of the river, the in-situ CO₂
101 concentrations combined with discrete sampling for dissolved CH₄, DOC, DIC, total bacterial number and
102 particulate organic matter. These measurements were complemented with regular floating chamber
103 measurements of CO₂ emission fluxes. We performed these observations during two main open water seasons
104 of the year - the peak of the spring flood and the end of the summer baseflow. Our first objective was to
105 quantify the difference in C concentration and emission during two seasons for the main stem and the
106 tributaries and to relate these differences to main physico-chemical parameters of the water column and
107 physio-geographical parameters (land cover) of the river watersheds. Our second objective was to obtain total
108 C emission flux from the river watershed area and compare it to downstream export yield of dissolved and
109 particulate carbon.

110

111

112

113

114 2. Study Site, Materials and Methods

115 2.1. Ket River and its tributaries

116 The Ket River main stem and its 26 tributaries sampled in this study include watersheds of distinct
117 sizes (catchment area ranged from 94,000 at the Ket's mouth to 20 km² of smallest tributary), but rather
118 similar lithology, climate and vegetation (**Fig. 1, Table S1**). This poorly accessible river basin is fully pristine
119 (50 % forest, 40 % wetlands), and has almost no agricultural and forestry activity. The watershed of Ket has
120 very low population density (0.27 person km⁻²) and lacks road infrastructure due to absence of oil and gas
121 development and production. In this regard, this river can serve as a model for medium size bog-forest rivers
122 of the western Siberia Lowland and results obtained from this watershed can be extrapolated to much larger
123 territory, comprising about 1 million km² of permafrost-free taiga forest and bog regions of the southern part
124 of WSL.

125 The mean annual air temperatures (MAAT) is -0.7 ± 0.1 °C and the mean annual precipitation is 520
126 ± 20 mm y⁻¹ in the central part of the basin. The lithology of this part of western Siberian lowland is dominated
127 by Pleistocene silts and sands with carbonate concretions overlaid by quaternary deposits (loesses, fluvial,
128 glacial and lacustrine deposits). The dominant soils are podzols in forest areas and histosols in peat bog
129 regions. Further description of climate, lithology and landscape features of the territory is provided in former
130 studies (Frey and Smith, 2007; Pokrovsky et al., 2015).

131 The peak of annual discharge in 2019 occurred in the end of May; in August, the discharge was 3 to
132 5 times smaller (**Fig. 1**). Note that low runoff, lack of relief and highly homogenous landscape coverage of
133 the permafrost-free zone of western Siberia in general and of the Ket River basin in particular provide quite
134 smooth hydrographs of the rivers. In this regard, the spring flood period is extended over 2 months, from the
135 beginning of May to middle of July, whereas summer baseflow includes second half of July, August and
136 September. As a result, similar to previous study of rivers along a 2500 km transect of the WSL territory, the
137 timing of the two sampling campaigns covered approximately 80% of the annual water discharge in the basins
138 (Serikova et al., 2018). From May 18 to May 28, 2019, and from August 30 to September 2, 2019, we started
139 the boat trip in the middle course of the Ket River (Beliy Yar), and moved, first, 475 km upstream the Ket
140 river till its most headwaters, and then moved 834 km downstream till the river mouth, with an average speed

141 of 20 km h⁻¹. During summer baseflow, the 4-days trip was shortened by 200 km due to too low water level
142 in the upper reaches of the main stem and some small tributaries. We stopped each 30-50 km along the Ket
143 River and sampled for major hydrochemical parameters, GHG, river suspended matter and total bacterial
144 number of the main stem. We also moved several km upstream of selected tributaries to record CO₂
145 concentrations for at least 1 h and to sample for river hydrochemistry. At several occasions during spring
146 flood, we monitored CO₂ concentration and performed chamber measurements in the main stem and
147 tributaries during both day and night time period.

148

149 *2.2. CO₂ and CH₄ concentrations and CO₂ fluxes by floating chambers*

150 Surface water CO₂ concentration was measured continuously, *in-situ* by deploying a portable infrared
151 gas analyzer (IRGA, GMT222 CARBOCAP® probe, Vaisala®; accuracy ± 1.5%) of two ranges (2 000 and
152 10 000 ppm) as described in previous work of our group on the Lena River (Vorobyev et al., 2021). Sensor
153 preparation was conducted in the lab following the method described by Johnson et al. (2009). The
154 measurement unit (MI70, Vaisala®; accuracy ± 0.2%) was connected to the sensor allowing instantaneous
155 readings of *p*CO₂. The sensors were calibrated in the lab against standard gas mixtures (0, 800, 3 000, 8 000
156 ppm; linear regression with R² > 0.99) before and after the field campaign. The sensors' drift was 0.03-0.06%
157 per day and overall error was 4-8% (relative standard deviation, RSD). Following calibration, post-
158 measurement correction of the sensor output induced by changes in water temperature and barometric
159 pressure was done by applying empirically derived coefficients following Johnson et al. (2009). These
160 corrections never exceeded 5% of the measured values. During the cruise, we routinely measured atmospheric
161 CO₂ with the probe as a check for its good functioning. Furthermore, we tested two different sensors in several
162 sites of the river transect: a main probe used for continuous measurements and another probe used as a control
163 and never employed for continuous measurements. We did not find any sizable (>10%) difference in
164 measured CO₂ concentration between these two probes.

165 The probe was enclosed within a waterproof and gas-permeable membrane. For this, we used a
166 protective expanded polytetrafluoroethylene (PTFE) sleeve that is highly permeable to CO₂ but impermeable
167 to water (Johnson et al., 2009). The sensor was placed into a tube which was submerged 0.5 m below the

168 water surface. A Campbell logger was connected to the system allowing continuous recording of the CO₂
169 concentration, water temperature and pressure every minute. These readings were averaged over 10 minute
170 intervals yielding 732 individual pCO₂, water temperature and pressure values. The CO₂ concentrations in the
171 Ket River tributaries included between 10 and 20 averaged pCO₂ values for each tributary (250 measurements
172 in total) during spring flood period. In addition to continuous *in-situ* CO₂ measurements, we estimated pCO₂
173 via measured pH and DIC values, using the set of constants typically applied for riverine pCO₂ estimation in
174 organic-rich waters (Cai and Wang, 1998; DelDuco and Xu, 2017). The U-test (Mann-Whitney) demonstrated
175 a lack of significant difference in CO₂ concentrations measured by Vaissala and calculated from the pH and
176 DIC of the river water.

177 For CH₄ analyses, unfiltered water was sampled in 60-mL Serum bottles. For this, the bottles and caps
178 were manually submerged at approx. 30 cm depth from the water surface. The bottles were closed without
179 air bubbles using vinyl stoppers and aluminum caps and immediately poisoned by adding 0.2 mL of saturated
180 HgCl₂ via a two-way needle system. The samples were stored approximately one week in the refrigerator
181 before the analyses. In the laboratory, a headspace was created by displacing approximately 40% of water
182 with N₂ (99.999%). Two 0.5-mL replicates of the equilibrated headspace were analyzed for their
183 concentrations of CH₄, using a Bruker GC-456 gas chromatograph (GC) equipped with flame ionization and
184 thermal conductivity detectors (Serikova et al., 2019; Vorobyev et al., 2021). After every 10 samples, a
185 calibration of the detectors was performed using Air Liquid gas standards (i.e. 145 ppmv). Duplicate injection
186 of the samples showed that results were reproducible within ±5%. The specific gas solubility for CH₄
187 (Yamamoto et al., 1976) were used in calculation of the CH₄ content in the water.

188 Discrete CO₂ fluxes were measured by using two floating CO₂ chambers equipped with non-
189 dispersive infrared SenseAir® CO₂ loggers (Bastviken et al., 2015), at each of the 7 (spring flood) and 6
190 (summer baseflow) sampling location of the main stem and 26 tributaries following the procedures described
191 elsewhere (Serikova et al., 2019; Krickov et al., 2021). The chambers were not anchored but slowly free-
192 drifted together with the boat, because it is known that anchored chambers can artificially enhance fluxes due
193 to turbulence thus providing erroneous estimates (Lorke et al., 2015). The CO₂ accumulation rate inside each
194 chamber was recorded continuously at 300 s interval. We used first 0.5–1 h of measurements for computing

195 CO₂ accumulation rate inside each chamber by linear regression. In addition to *in-situ* chamber measurements,
196 CO₂ fluxes were calculated from wind speed and surface water gas concentrations using standard approaches
197 (Guérin et al., 2007; Wanninkhof, 1992; Cole and Caraco, 1998). This technique is based on the two-layer
198 model of Liss and Slater (1974), and widely used for GHG flux assessment (Repo et al. 2007; Laurion et al.
199 2010; Elder et al. 2018). The gas transfer coefficient was taken from Cole and Caraco (1998):

$$200 \quad k_{600} = 2.07 + 0.215 \cdot U_{10}^{1.7} \quad (1)$$

201 where U_{10} is the wind speed taken at 10 m height. Average daily wind speed was retrieved from official data
202 of the nearest weather station (Belyi Yar town) as published by Rosgidromet for the day of sampling. The
203 gas transfer velocity was calculated in two ways - assuming zero wind speed and the actually measured wind
204 speed at the site of sampling or at the Belyi Yar town, middle course of the Ket River. For comparison with
205 previous estimates in large Siberian rivers (Karlsson et al., 2021; Vorobyev et al., 2021), we also used a gas
206 transfer velocity of 4.46 m d⁻¹ measured in the 4 largest rivers of Western Siberia Lowland (WSL) in June
207 2015 (Ob', Pur, Pyakupur and Taz rivers, Karlsson et al., 2021) which is representative for large lowland
208 rivers (Alin et al., 2011; Beaulieu et al., 2012).

209

210 *2.3. Chemical analyses of the river water*

211 The dissolved oxygen (CellOx 325; accuracy of ±5%), specific conductivity (TetraCon 325; ±1.5%),
212 and water temperature (±0.2 °C) were measured in-situ at 20 cm depth using a WTW 3320 Multimeter. The
213 pH was measured using portable Hanna instrument via combined Schott glass electrode calibrated with
214 standard buffer solutions (4.01, 6.86 and 9.18 at 25°C), with an uncertainty of 0.01 pH units. The temperature
215 of buffer solutions was within ± 2°C of that of the river water. The water was sampled in pre-cleaned
216 polypropylene bottle from 20-30 cm depth in the middle of the river and immediately filtered through
217 disposable single-use sterile Sartorius filter units (0.45 µm pore size). The first 50 mL of filtrate was
218 discarded. The DOC and Dissolved Inorganic Carbon (DIC) were determined by a Shimadzu TOC-VSCN
219 Analyzer (Kyoto, Japan) with an uncertainty of 3% and a detection limit of 0.1 mg/L. Blanks of MilliQ water
220 passed through the filters demonstrated negligible release of DOC from the filter material. The SUVA was

221 measured via ultraviolet absorbance at 254 nm using a 10-mm quartz cuvette on a Bruker CARY-50 UV-VIS
222 spectrophotometer.

223 The concentration of C and N in suspended material (Particulate Organic Carbon and Nitrogen (POC
224 and PON, respectively)) was determined via filtration of 1 to 2 L of freshly collected river water (at the river
225 bank or in the boat) with pre-weighted GFF filters (47 mm, 0.45 μm) and Nalgene 250-mL polystyrene
226 filtration units using a Mityvac® manual vacuum pump. Particulate C and N were measured using catalytic
227 combustion with Cu-O at 900°C with an uncertainty of $\leq 0.5\%$ using Thermo Flash 2000 CN Analyzer at
228 EcoLab, Toulouse. The samples were analyzed before and after 1:1 HCl treatment to distinguish between
229 total and inorganic C; however the ratio of $C_{\text{organic}} : C_{\text{carbonate}}$ in the river suspended matter (RSM) was always
230 above 20 and the contribution of carbonate C to total C in the RSM was equal in average $0.3 \pm 0.3\%$ (2 s.d., n
231 = 30).

232 Total microbial cell concentration was measured after sample fixation in glutaraldehyde, by a flow
233 cytometry (Guava® EasyCyte™ systems, Merck). Cells were stained using 1 μL of a 10 times diluted SYBR
234 GREEN solution (10000x, Merck), added to 250 μL of each sample before analysis. Particles were identified
235 as cells based on green fluorescence and forward scatter (Marie et al., 2001).

236

237 *2.4. Riverine carbon export flux by the Ket catchment*

238 The C export flux over active (unfrozen) period (May to October) from the Ket basin was calculated
239 based on monthly-averaged discharge at the river mouth in 2019 available from Russian Hydrological Survey
240 and DOC, DIC and POC concentrations measured in the low reaches of the Ket River in this study (see
241 hydrograph in **Fig. 1**). Riverine element fluxes should be usually estimated using a LOADEST method
242 (Holmes et al., 2012) from calculated daily element loads. The latter typically obtained from a calibration
243 regression, applied to daily discharge. This calibration regression can be constructed from time series of
244 paired streamflow and measured element concentration data for sufficient period of the year. In our previous
245 works in this and other similar boreal regions, we demonstrated that this method provides reasonable (within
246 10 to 30 %) agreement with monthly export fluxes calculated by multiplying mean monthly discharge by
247 mean monthly concentration (Chupakov et al., 2020; Pokrovsky et al., 2022; Vorobyev et al., 2019). Given

248 that the intrinsic uncertainties on mean monthly discharge are also between 10 and 20 % (see discussion for
249 the WSL rivers in Pokrovsky et al., 2020), in this study, for open-water period export flux calculation, we
250 used DOC, DIC and POC concentrations measured during spring flood (for May and June period) and
251 baseflow (for August, September and October period). For the month of July, we used the mean
252 concentrations of end of May and August-September which is in accord with seasonal discharge pattern of
253 the Ket River. Note that the contribution of non-studied October month to total open water period water flux
254 is < 10 % and thus cannot provide sizable uncertainties

255

256 *2.5. Landscape parameters and water surface area of the Ket River basin*

257 The physio-geographical characteristics of the 26 Ket tributaries and the 7 points of the Ket main stem
258 (**Table S1, Fig. S1**) were determined by applying available digital elevation model (DEM GMTED2010),
259 soil, vegetation and lithological maps. The landscape parameters were typified using TerraNorte Database of
260 Land Cover of Russia (Bartalev et al., 2020; <http://terranorte.iki.rssi.ru>). This included various type of forest
261 (evergreen, deciduous, needleleaf/broadleaf), grassland, tundra, wetlands, water bodies and riparian zones.
262 Note that the land cover data correspond to the whole catchment area upstream of the sampling point. The
263 climate parameters the watershed were obtained from CRU grids data (1950-2016) (Harris et al., 2014) and
264 NCSCD data (Hugelius et al., 2013), respectively. The biomass was obtained from BIOMASAR2 dataset in
265 raster format with spatial resolution of 1 x 1 km (Santoro et al., 2010). The soil OC content was taken from
266 the Northern Circumpolar Soil Carbon Database (NCSCD). The original NCSCD dataset produced in GIS
267 vector format corresponding to 1:1,000,000 scale of topographic map. It could be rasterized to 1 x 1 km pixel
268 resolution. The lithology layer was taken from GIS version of Geological map of the Russian Federation
269 (scale 1:5,000,000, <http://www.geolkarta.ru/>). We quantified river water surface area using the global SDG
270 database with 30 m² resolution (Pekel et al., 2016) including both seasonal and permanent water for the open
271 water period of 2019 and for the multiannual average (reference period 2000-2004). We also used a more
272 recent GRWL Mask Database which incorporates first order temporary non-active streams (Allen and
273 Pavelsky, 2018).

274

275 2.6. *Data analysis*

276 Carbon concentrations and fluxes for all dataset were tested for normality using a Shapiro-Wilk test.
277 In case if the data were not normally distributed, we used non-parametric statistics. Comparisons of GHG
278 parameters in the main stem and tributaries during two sampling seasons were conducted using a non-
279 parametric Mann Whitney test at a significance level of 0.05. For comparison of unpaired data, a non-
280 parametric H-criterion Kruskal-Wallis test was used to reveal the differences between different study sites.
281 The Pearson rank order correlation coefficient ($p < 0.05$) was used to determine the relationship between CO₂
282 concentrations and emission fluxes and main landscape parameters of the Ket River tributaries, as well as
283 other potential drivers such as pH, O₂, water temperature, specific conductivity, DOC, DIC, particulate carbon
284 and nitrogen, and total bacterial number.

285 Further identification of C pattern drivers in river waters included a Principal Component Analysis
286 which allowed to test the effect of various hydrochemical and landscape parameters on CO₂ and CH₄
287 concentrations and CO₂ emissions. In addition to PCA, a Redundancy analysis (RDA) was used to extract
288 and summarize the variation in C pattern that can be explained by a set of explanatory variables
289 (environmental, climatic and hydrochemical factors). The RDA combines a PCA and multiple regression
290 analysis and it was run in XLSTAT is a statistical software that works as an add-on to Excel.

291

292

293 **3. Results**

294 *3.1. Greenhouse gases and dissolved and particulate C*

295 The main hydrochemical parameters and greenhouse gases concentration and exchange fluxes of the
296 Ket River and its tributaries are listed in **Table 1** and primary data are provided in **Table S2** of the
297 Supplement. Continuous pCO₂ measurements in the main stem during the spring (764 individual data points
298 over the full distance of the boat route (834 km), demonstrated a lack of systematic change in CO₂
299 concentration from headwaters to the mouth. The CO₂ concentration in tributaries was generally higher than
300 that in the main stem. As a result, the pCO₂ changed by a factor of 1.5 to 2 when tributaries with high CO₂
301 concentrations join the main stem (**Fig. 2 A**). There were strong but non-systematic variations in CO₂

302 concentration in the tributaries during the summer (**Fig. 2 C**). The CH₄ concentration (**Table 1 and Fig. S2**
303 **A, B**) was low in the Ket River (around 0.17 and 0.86 μmol L⁻¹ in May and August, respectively) and in the
304 tributaries (range 0.09 to 2.57 μmol L⁻¹, 2 to 3 times higher values during the baseflow). These values are
305 consistent with the range of CH₄ concentration in other Siberian Rivers such as Lena (0.03 to 0.199 μmol L⁻¹,
306 ¹, Bussman, 2013; Vorobyev et al., 2021). In the Ket River main stem and tributaries, the CH₄ concentrations
307 are 300-2000 and 100-150 times lower than those of CO₂ during spring and summer, respectively, and ranged
308 from 0.05 to 2.0 μmol L⁻¹. Consequently, diffuse CH₄ emissions (**Table 1, Fig. S2 C, D**) constituted 0.1 to
309 0.5% of total C emissions and are not discussed in further detail.

310 During spring flood, CO₂ fluxes ranged from 0.26 to 3.2 g C m⁻² d⁻¹ in the main stem and tributaries
311 (**Table 1; Fig. 2 B**). During baseflow, the flux in the tributaries varied from 0.37 to 7.4 g C m⁻² d⁻¹ and was a
312 factor of 2 to 3 higher than that in the main stem (**Fig. 2 D; Table 1**). The CO₂ concentration in the river
313 water and gas transfer velocity assessed from discrete measurements by floating chambers ($K_T = 0.08-1.83$
314 m d⁻¹ in the main stem; 0.2-1.86 m d⁻¹ in the tributaries, **Table 1**) allowed for calculation of the continuous
315 CO₂ fluxes (**Fig. 2 B**). For this, we used an average value of K_T between two chamber sites (separated by a
316 distance of 50 to 100 km) to calculate the FCO₂ from in-situ measured pCO₂ in the river section between
317 these two sites. Note that the wind calculated flux was 1.5 to 2 times higher than that measured by chambers,
318 although in 30 % of cases, the wind-speed calculated fluxes were similar to or lower than those measured by
319 floating chambers. The calculation with $K_T = 4.46$ m d⁻¹ (the value typical for large Siberian rivers)
320 overestimated the flux by a factor of 3.7 to 6.0 (**Table S2** of the Supplement). In both cases, the overestimation
321 of calculated flux relative to chamber-measured flux was most pronounced in the tributaries rather than in the
322 main stem.

323 The DIC concentration increased 5 to 10 times between the spring (2.4 to 2.8 mg L⁻¹) and summer
324 baseflow (18 to 20 mg L⁻¹) and the pH increased by 0.5-0.7 units between spring freshet and summer baseflow
325 (**Fig. 3 and Fig. S3 A, B** of the Supplement). The DOC concentration ranged from 18 to 25 mg L⁻¹ during
326 flood and from 15 to 18 mg L⁻¹ during baseflow (**Fig. 3**). There was no systematic variations in DOC
327 concentration over the 834 km of the main stem (20.7 ± 3.6 and 15.0 ± 1.4 mg L⁻¹ in May and August,
328 respectively); however, it was slightly higher and more variable in the tributaries (22.0 ± 4.0 and 16.5 ± 7.4

329 mg L⁻¹, **Fig. S3 C, D**). The SUVA₂₅₄ remained highly stable throughout the seasons for both the tributaries
330 and the main stem (range from 4.2 to 4.9 L mg C⁻¹ m⁻¹, **Table 1**). The POC was 3 times higher during baseflow
331 compared to spring and ranged from 2 to 10 mg L⁻¹ (**Fig. 3** and **Fig. S3 E, F**). The total bacterial number
332 ranged from 5.0×10^5 to 8.7×10^5 cells mL⁻¹ for the main stem and tributaries without significant ($p > 0.05$)
333 seasonal variation (**Fig. 3** and **S3 G, H**).

334

335 *3.2. Diurnal and spatial variation in CO₂ concentration and flux*

336 The diel (day/night) measurements of CO₂ concentrations have been performed on six tributaries of
337 the Ket River during the spring flood period (**Fig. 4**). In two of them (Sochur ad Lopatka), we measured both
338 CO₂ concentration and CO₂ fluxes via floating chambers. Continuous CO₂ concentrations exhibited a
339 variation between 5 and 25% of the average value. Only in the case of a small tributary Segondenka (**Fig. 4**
340 **E**), when we measured CO₂ over 38 h, there was a local maximum in concentration between 6 and 7 pm
341 during the first and second day of monitoring, without any significant link to the water temperature. The
342 deviation of FCO₂ from the average value over the period of observation in two tributaries (**Fig. 4 A, B**) did
343 not exceed 20%, without any detectable difference between day and night period.

344 The spatial variation in pCO₂ and FCO₂ were tested during spring time in the flood zone of the Ket
345 River middle course, where the flood zone was connected to the main channel. Regardless of the distance
346 from the main stem and the size of the water body, the variation in pCO₂ and chamber-based fluxes were
347 within 30% of the values measured in the main stem. This suggests that the main stem parameters can be used
348 for upscaling the C emissions to the overall flood plain during May, provided that the water bodies are
349 connected to the rivers. Further tests of spatial variation were performed on selected small tributaries, when
350 we moved 8 to 16 km upstream towards the headwaters and monitored the CO₂ concentration in the river
351 water. There was no sizable trend in CO₂ concentration over several km length of the tributary, consistent
352 with small fluctuations over the hundred km-scale of the main stem (**Fig. S4 A**). Altogether, rather minor
353 spatial and diel variations in both CO₂ concentration and emission fluxes support the chosen sampling strategy
354 and allow reliable extrapolation of obtained results to full surface of lotic waters of the Ket River basin, during
355 open water period.

356 *3.3. Impact of water chemistry and catchment characteristics on CO₂ concentrations and emissions*

357 There were generally no strong correlations between CO₂ and CH₄ and the main parameters of the
358 water column (DOC, DIC, POC, TBC and SUVA (**Table 2**)). The CO₂ concentration negatively correlated
359 with O₂ concentration ($R_{\text{Pearson}} = -0.68$, $p < 0.05$) and FCO₂ positively correlated with SUVA₂₅₄ ($R = 0.34$, p
360 < 0.05), **Fig. 5 A, B**. Other hydrochemical characteristics of the water column did not impact CO₂ and CH₄
361 concentration and CO₂ flux. During spring flood, there was no positive correlation between FCO₂ of the river
362 water and various hydrochemical characteristics. During the summer baseflow, there were positive
363 correlations between CO₂ concentration or flux and SUVA and total bacterial number (**Table 2**).

364 Among different landscape factors, only deciduous light needleleaf forest (larch trees) exhibited
365 significant ($p < 0.01$) positive correlations ($0.6 \leq R_s \leq 0.7$) with CO₂ concentration and flux of the Ket River
366 main stem and tributaries, detectable only during the summer baseflow period (**Fig. 5 C**). The peatland and
367 bogs at the watershed exhibited only weak, although positive ($0.2 < R_s < 0.4$), correlation with pCO₂ and
368 FCO₂ (**Table 2**). The other potentially important landscape factors of the river watershed (type of forest,
369 riparian and total aboveground vegetation, recent burns, water bodies) as well as lithological parameters
370 (clays, silts, sands with or without of the presence of carbonate concretions) did not significantly impact the
371 CO₂ and CH₄ concentration and measured CO₂ fluxes in the Ket River basin (**Table 2**). The mean annual
372 precipitation (MAP) at the watershed positively correlated with pCO₂ and FCO₂ during the baseflow (**Fig. 5**
373 **D**).

374 Principal Component Analysis (PCA) demonstrated a general lack of control of physico-chemical
375 parameters of the water column and watershed land cover on C emission pattern in the river waters. The PCA
376 identified two factors that had generally low ability to describe the variance (19 and 7%, respectively; **Table**
377 **S3** of the Supplement). None of the factors acted significantly on dissolved CO₂, CH₄ or CO₂ flux in the river
378 water. The RDA treatment did not provide additional insights into environmental control of C pattern across
379 the rivers and seasons. After normalization, the main result was that the analyses are not statistically
380 significant ($p > 0.05$).

381

382

383

384 *3.4. Areal C emissions and export fluxes*

385 The C emissions ($> 99.5\%$ CO_2 , $< 0.5\%$ CH_4) from the lotic waters of the Ket River basin were
386 assessed based on total river water coverage of the Ket watershed in 2019 (856 km^2 , of which 691 km^2 is
387 seasonal water, according to the Global SDG database). Given that the measurements were performed at the
388 peak of spring flood in 2019, we used the maximal water coverage of the Ket River basin to calculate the
389 emissions during May and June, and baseflow measurements for July-October period.

390 For C emission calculation, we used the mean values of FCO_2 of the main stem and the tributaries
391 ($1.31 \pm 0.81 \text{ g C m}^{-2} \text{ d}^{-1}$ for spring flood; $2.11 \pm 1.86 \text{ g C m}^{-2} \text{ d}^{-1}$ for summer-autumn baseflow) which covers
392 full variability of both tributaries and the Ket River main channel (**Table 1, Figure 3**). For the month of July
393 which was not sampled in this work and which represents a transition period between the flood and the
394 baseflow, we used the mean value of May and August ($1.55 \text{ g C m}^{-2} \text{ d}^{-1}$). For the two months of maximal
395 water flow (May - June), the C emission from the whole Ket basin amounts to $68 \pm 42 \text{ Gg}$. When summed up
396 with July ($25 \pm 20 \text{ Gg}$) and summer-autumn baseflow period (August to October) emission ($32 \pm 28 \text{ Gg}$), the
397 total open water season emission flux is 125 Gg . The uncertainty on the total emission over 6 months of the
398 open water period is difficult to quantify but it can be estimated as between 30 and 50 %. This range covers
399 both the uncertainty of the water coverage of the territory (i.e., Krickov et al., 2021) and the seasonal and
400 spatial variations of CO_2 emission in the Ket basin assessed in the present study.

401 Based on yield calculations described in section 2.4, the total annual (excluding ice-covered period)
402 riverine C export from the Ket River basin ($S_{\text{watershed}} = 94,000 \text{ km}^2$) is 0.35 Tg ($3.7 \text{ t C km}^{-2}_{\text{land}} \text{ y}^{-1}$), of which
403 DOC, DIC and POC accounts for 56, 24 and 20%, respectively. Therefore, over the 6 month of open water
404 period, the C emissions from lotic waters of Ket watershed constituted less than 30% of the dissolved and
405 particulate downstream export of carbon.

406

407

408

409

410 4. DISCUSSION

411 4.1. Temporal and spatial pattern of CO₂ emissions from the river waters

412 The first important result of the present study is quite low spatial and seasonal variability in both CO₂
413 concentration and emissions, as well as in DOC concentration and aromaticity (reflected by SUVA₂₅₄) in the
414 main channel (**Fig. 3, S3, Table 1**). The variability in the tributaries was much larger, with differences in
415 dissolved and gaseous C parameters between spring flood and summer-autumn baseflow (**Table S4 A**). While
416 CO₂ concentrations were different between tributaries and the main stem during both flood and baseflow, the
417 CO₂ flux was not different between the main stem and tributaries regardless of season (**Table S4 B**). This,
418 together with lack of diel variations in CO₂ concentrations and emissions during spring period of maximal
419 water coverage (**Fig. 4**), suggest rather stable pattern of CO₂ in the river water, not linked to short-scale
420 processes (primary productivity, photolysis, daily temperature variation). Indeed, negligible primary
421 productivity in the water column may stem from low water temperatures (9.3 °C), shallow photic layer of
422 organic-rich waters (DOC of 22 mg L⁻¹) and lack of periphyton activity during high flow of the spring flood.
423 Note that this finding contrasts the recent results of high frequency pCO₂ measurements in temperate rivers
424 that show a 30 % higher nocturnal emission compared to daytime observations (Gómez-Gener et al., 2021b).
425 At the same time, several studies in tropical DOM-rich rivers such as Congo (Borges et al. 2019) have not
426 detected diel variations of CO₂ because aquatic pelagic primary production was low (Descy et al., 2018) due
427 to strong light attenuation in the water column by DOM.

428 Concerning spatial variability of C concentrations and emissions during the spring flood, the pCO₂
429 did not demonstrate sizable variation along the main stem of the Ket River and some of its tributaries, when
430 moving from the mouth to the headwaters. The SUVA also remained highly stable along the river flow. This,
431 together with a lack of FCO₂ correlation with river watershed area during this period (**Table 2**), suggest
432 relatively modest control of headwater C cycling by ‘fresh’ unprocessed organic matter from upland mire
433 waters on CO₂ emissions from the Ket River tributaries. Much stronger control of mire waters is reported in
434 boreal zone of the Northern Europe (Wallin et al., 2013, 2018). Furthermore, our results on the Ket River
435 main stem and tributaries are in contrast to the general view of disproportional importance of headwater
436 streams in overall CO₂ emission from river basins (Li et al., 2021). A likely explanation is relative low values

437 of gas transfer velocity measured in the small streams of the Ket basin in this study (0.2 - 2.0 m d⁻¹, **Table 1**).
438 Although these values are totally consistent with transfer coefficients for western Siberia calculated by Liu et
439 al. (2022) based on reach-slope and flow velocity (i.e., ≤ 2 m d⁻¹), they are typical of lakes rather than rivers
440 (i.e., Kokic et al., 2015) and stem from low flow rate, strongly forested and wind-protected river bed without
441 distinct valley due to generally flat orographic context of this part of the WSL (Serikova et al., 2018).

442 It is worth noting that the overestimation of calculated flux relative to chamber-measured flux was
443 most pronounced in the tributaries rather than in the main stem. Overall, due to small size and short fetch of
444 the Ket River and its tributaries (see pictures of typical environments in **Fig. S4 B-D** of the Supplement), we
445 believe that lower values of K_T are more pertinent to the studied river basin, which has extended flood zone.
446 This is consistent with observations in other flooded regions, where a canopy of vegetation protects the water-
447 air interface from wind stress thus rendering the gas transfer velocity lower compared to open water such as
448 large river (i.e., Foster-Martinez and Variano, 2016; Ho et al., 2018; Abril and Borges, 2019). We therefore
449 warn against the use of high value of transfer velocity, suitable for large rivers of the boreal zone, for assessing
450 the emissions in medium and small size, sheltered streams with extensive riparian vegetation. Another
451 important aspect linked to C emissions from flooded forest (notably birch trees, see **Fig. S4 B**) of the
452 floodplain (e.g. Pangala et al., 2017), not investigated in this study.

453

454 *4.2. Environmental factors possibly controlling CO₂ concentration and emission pattern in the Ket* 455 *River main stem and tributaries*

456 Despite sizable variability of pCO₂ in the tributaries, especially during the baseflow, there were no
457 correlations between either pCO₂ or FCO₂ and main hydrochemical parameters of the water column (**Table**
458 **2**). The only exception is O₂ concentration, which negatively correlated with pCO₂ during spring flood and
459 both pCO₂ and FCO₂ during summer baseflow (**Fig. 5 A**). This finding suggests potential importance of
460 shallow suboxic riparian flooded zone, meadows and forest, as well as floodplain lakes, in controlling CO₂
461 build up in the water column due to diffusion from sediments or decaying macrophytes, as it was shown for
462 the floodplain of the Ob River middle course (Krickov et al., 2021). We believe that main reasons of
463 remarkable stability in CO₂ concentrations and emissions and weak environmental control on dissolved and

464 gaseous pattern in the Ket River basin are (1) essentially homogeneous landscapes, lithology and quaternary
465 deposits of the whole river basin (20-25 % bogs, 60-70% forest, 3-5 % riparian zone), and (2) strong
466 dominance of allochthonous sources in both dissolved and particulate organic matter. Indeed, the SUVA and
467 bacterial number (TBC) positively correlated with both $p\text{CO}_2$ and FCO_2 during summer (**Fig. 5 B; Table 2**),
468 which may indicate non-negligible role of bacterial processing of allochthonous (aromatic) DOC delivered
469 to the water column from wetlands and mires. As such, homogeneous land cover and essentially
470 allochthonous DOC can still lead to variations of CO_2 per stream size, with small systems showing higher
471 values than large systems as predicted conceptually (Hotchkiss et al., 2015) and verified at basin-scale (e.g.
472 Borges et al., 2019). Consistent with this, we observed systematically higher CO_2 concentration and flux in
473 small tributaries [which were fed by mire waters with ‘non-processed’ OM] compared to the main stem
474 (**Table 2**). Furthermore, the positive correlation between mean annual precipitation (MAP) and $p\text{CO}_2$ and
475 FCO_2 during the baseflow (**Table 2, Fig. 5 D**) could reflect the importance of water storage in the mires and
476 wetlands (which also showed positive but less significant correlations, **Table 2**) during the summer time, and
477 progressive release of CO_2 and DOC-rich waters from the wetlands to the streams. Another indirect evidence
478 of the mire water control on CO_2 emission from the river comes from daily CO_2 pattern in a tributary of the
479 Ket River (**Fig. 4 E**). For this relatively small river ($S_{\text{watershed}} = 472 \text{ km}^2$), we noted that there was quite heavy
480 rainfall, between 7 am and 3 pm, prior to the CO_2 peak which was observed at 7 pm. Given that water
481 residence time is very short during spring flood, when the soils are partially frozen, the delivery of
482 allochthonous DOM and elevated CO_2 from adjacent mires could be the cause of observed CO_2 peak.
483 Generally, the terrestrial source controlling CO_2 pattern in the Ket River could be either soil litter leachates
484 (in spring) or bog water (during baseflow, when the river water is substantially derived from wetlands, Ala-
485 aho et al., 2018a, b). Therefore, the patterns in CO_2 emissions observed in the present study during summer
486 baseflow thus suggest the importance of allochthonous organic matter from the peatland for CO_2 production
487 in the water column and in soils where the degradation of DOC is enhanced by the presence of bacteria. This
488 is consistent with observations in other regions that, during summer-time, numerous processes contribute to
489 increase CO_2 in rivers such as higher temperature stimulating microbial metabolism, longer residence time
490 and enhanced flow paths of soil water (Borges et al. 2018).

491 A correlation between CO₂ flux during baseflow and the proportion of deciduous needleleaf forest at
492 the watershed (**Fig. 5 C**) may suggest the importance of C cycling by larch trees and their possible control on
493 the delivery of degradable organic matter to the river. Similar control of larch vegetation on riverine CO₂ has
494 been suggested for the Lena River, Eastern Siberia (Vorobyev et al., 2021) although we acknowledge that
495 further observations on contrasted Siberian watersheds are necessary to confirm the observation that larch
496 trees litterfall led to export of degradable OM to the river.

497 In the Ket River basin, the local soil/groundwater effects are expected to be more pronounced during
498 baseflow, due to lower impact of dilution, compared to the spring flood period. The hypothesis of deeper flow
499 path in summer compared to spring is confirmed for the WSL (Frey and McClelland, 2009; Pokrovsky et al.,
500 2015; Serikova et al., 2018) and is supported in this study by a strong increase in DIC concentration between
501 spring and summer (**Fig. 3**). Thus, although the pairwise correlations between parameters do not support any
502 particular mechanism, it is not excluded that OM bio- and photo degradation and local mire water feeding
503 drive FCO₂ in spring, and that deeper flowpaths and DIC export drive the elevated FCO₂ in summer. The
504 latter is consistent with results of analysis of streams and rivers across the contiguous United States, which
505 demonstrated that ~60% of CO₂ evasion is from external sources rather than internal production (Hotchkiss
506 et al., 2015). In view of lack of correlation of CO₂ emissions in the Ket River and tributaries with
507 hydrochemical parameters of the water column, we believe that external source of CO₂ in studied river system
508 represents sizable contribution to total riverine CO₂ evasion across the seasons and sampling sites. In
509 particular, in small peatland streams, the CO₂-rich deep peat/groundwater is known to be the major source of
510 aquatic CO₂ under low flow conditions (Dinsmore and Billett, 2008), whereas in boreal headwater streams
511 of N Sweden the main source of stream CO₂ was inflowing CO₂-rich soil waters (Winterdahl et al., 2016).

512 Another important factor responsible for higher CO₂ production in the water column in summer
513 compared to spring could be POC degradation. The riverine POC is known to be much more biodegradable
514 than DOC (Attermeyer et al., 2018), and the POC concentration in the Ket River basin increased 4-fold
515 between spring and summer (**Table 1**). The origin of summer-time POC and its lability remain elusive, but
516 could be a combination of plankton bloom and mire- or forest-derived DOC coagulation products in the water
517 column (Krickov et al., 2018). Furthermore, pronounced heterogeneity in CO₂ emission during baseflow

518 among tributaries may also reflect the heterogeneity of riverine organic matter which is known to be the
519 maximal during low flow conditions and minimal during high flow (Lynch et al., 2019).

520 The main unexpected result of this study is that none of the physiochemical parameters of the water
521 column and the land cover factor is sufficiently strong to drive the CO₂ and CH₄ patterns, although they show
522 pronounced spatial and seasonal variations. Although correlations do not necessary imply causation and some
523 correlations could be spurious or indirect, this analysis, together with PCA treatment, allow first order
524 assessment of possible governing factors or dismissing the environmental parameters that do not contribute
525 in GHG pattern control. A likely explanation is that simultaneous operation of multiple aquatic processes that
526 include carbon, oxygen, nutrient, and plankton and peryphyton dynamics as well as sediment respiration
527 control the CO₂ and CH₄ exchanges with the atmosphere, as it is known for boreal lakes and floodplain zones
528 of the boreal rivers (i.e., Bayer et al., 2019; Zabelina et al., 2021; Krickov et al., 2019). Given that even a
529 multiparametric statistical treatment (PCA) did not demonstrate sizable explanation capacity of the data set,
530 we cannot exclude that these potential physico-chemical, microbiological and landscape drivers are working
531 in different (opposing) directions and have counteracted each other. However, further in-depth analysis of
532 these interactions requires much better seasonal resolution, ideally over full period of the year, which was
533 beyond the scope of the present study.

534

535 *4.3. Emissions from the Ket River basin compared to downstream export of riverine carbon*

536 The estimated C emissions (> 99.5 % C; < 0.5 % CH₄) from the Ket River main channel over 830 km
537 distance (0.5 to 2.5 g C m⁻² d⁻¹) are comparable to those of the Ob River main channel (1.32±0.14 g C m⁻² d⁻¹
538 ¹ in the permafrost-free zone; Karlsson et al., 2021). The CO₂ emission in Ket's tributaries (1 to 2 g C m⁻² d⁻¹
539 ¹ in spring; 1 to 5 g C m⁻² d⁻¹ in summer) are within the range reported for small rivers and streams of the
540 permafrost-free zone of western Siberia (0 to 3.6 g C m⁻² d⁻¹ in spring; 4 to 9 g C m⁻² d⁻¹ in summer; Serikova
541 et al., 2018), forest and wetland headwater streams of northern Sweden (0.5 to 5 g C m⁻² d⁻¹; Gómez-Gener
542 et al., 2021a), and boreal streams in Canada and Alaska (0.8 to 5.2 g C m⁻² d⁻¹, Koprivnjak et al., 2010;
543 Teodoru et al., 2009; Crawford et al., 2013; Campeau et al., 2014). Total C emissions from the water surfaces
544 of the Ket River basin assessed in this study (148 g C-CO₂ m⁻²_{water} y⁻¹, assuming no emission under ice), when

545 normalized to the Ket river basin area ($S_{\text{watershed}} = 94,000 \text{ km}^2$), amounts to $1.35 \text{ g C m}^{-2}_{\text{land}} \text{ y}^{-1}$. Generally
546 higher land area - specific emissions, comparable or exceeding those of the Ket River, were reported in
547 Québec (1.0 to $4.6 \text{ g C m}^{-2} \text{ y}^{-1}$; Campeau and del Giorgio, 2014; Hutchins et al., 2019; Teodoru et al., 2009),
548 Sweden (1.6 to $8.6 \text{ g C m}^{-2} \text{ y}^{-1}$; Humborg et al., 2010; Jonsson et al., 2007; Lundin et al., 2013; Wallin et al.,
549 2011, 2018) and boreal portions of the Yukon River (7 to $9 \text{ g C m}^{-2} \text{ y}^{-1}$; Striegl et al., 2012; Stackpoole et al.,
550 2017). Possible reasons for these differences could be different areal coverage of the territory by river
551 network, the calculated rather than measured CO_2 fluxes, or the higher gas transfer velocity in the rivers from
552 mountainous regions.

553 The regional assessment of the Ket River basin performed in this study are based on direct chamber
554 measurements of emissions and as such provide rigorous basis for upscaling the CO_2 emissions from currently
555 understudied lotic waters of permafrost-free zone of Western Siberia. The C evasion from the fluvial network
556 of the Ket River assessed in the present work ($127 \pm 11 \text{ Gg y}^{-1}$, ignoring the emission during the ice breakup
557 in early spring) is 3 times lower than the total (DOC+DIC+POC) downstream export by this river from the
558 same territory (0.35 Tg C y^{-1}). The riverine C yield for the Ket River ($3.7 \text{ t C km}^{-2}_{\text{land}} \text{ y}^{-1}$) is in agreement
559 with regional C (DOC+DIC) yield by permafrost-free small and medium size rivers of the WSL (3 to 4 t C
560 $\text{km}^{-2}_{\text{land}} \text{ y}^{-1}$, Pokrovsky et al., 2020) and with the Ob River in the permafrost-free zone ($3.6 \text{ t C km}^{-2}_{\text{land}} \text{ y}^{-1}$,
561 Vorobyev et al., 2019). Note that the latter study of the Ob River, which is very similar in the environmental
562 context to the Ket River, included high frequency weekly sampling over several years of monitoring. Thus,
563 the similarity of downstream export fluxes of the Ket and Ob Rivers support the validity of approaches for
564 sampling and C yield calculation employed in the present study. Such high C yields in the southern,
565 permafrost-free part of the WSL stem from essentially inorganic carbon originated from groundwater
566 discharge of carbonate mineral rich reservoirs, abundant in this region (Pokrovsky et al., 2015). At the same
567 time, the organic C yield in rivers of this region is quite low and represents less than 20 % of total C yield
568 (Pokrovsky et al., 2020; Vorobyev et al., 2019). This can explain anomalously low value of C evasion : C
569 export of the Ket River ($1 : 3$) measured in this work as compared to the average values for permafrost-free
570 zone of Western Siberia ($1 : 1$, Serikova et al., 2019). One should also note that the gas transfer velocity
571 measured in this study provides much lower fluxes than those calculated with $K_T = 4.46 \text{ m d}^{-1}$ in previous

572 studies (**Table S2**). Another factor potentially leading to underestimation of C evasion in this study is GIS-
573 based minimal water coverage which does not include seasonal oxbow lakes, flooded forest and temporary
574 water bodies of the floodplain which provide sizable emissions (see Krickov et al., 2021). We also do not
575 exclude that some important hot moments / hot spots of C emission were missed in our sampling campaign,
576 such as summer baseflow/autumn peaks (Serikova et al., 2019) or stagnant zones of the floodplain in summer
577 (Krickov et al., 2021; Castro-Morales et al., 2021). This calls a need for higher spatial and temporal resolution
578 monitoring of C emission, with special focus on important events across full hydrological continuum.

579

580 **5. Concluding remarks**

581 Via combination of discrete floating chamber and hydrochemistry and continuous CO₂ concentration
582 measurements over 830 km of large pristine boreal river of western Siberia main channel and its 26 tributaries
583 during the peak of spring flood and the summer-autumn baseflow, we quantified spatial and temporal
584 variations, overall emissions of C (CO₂, CH₄) and export of (DOC, DIC and POC) during the 6 months of
585 open water period. The range of CO₂ and CH₄ concentrations in the main channel and tributaries as well as
586 CO₂ emissions were consistent with other boreal and subarctic regions but demonstrated rather low seasonal
587 and spatial variability. The diel CO₂ flux by floating chambers and continuous pCO₂ measurements in the
588 tributaries of the Ket River during spring flood demonstrated negligible impact of day/night period on the
589 CO₂ concentrations and emission fluxes.

590 We hypothesize that homogeneous landscape coverage (bog and taiga forest) provide stable
591 allochthonous input of DOM as confirmed by very weak spatial and seasonal variations of DOM aromaticity.
592 Among possible driving factors of CO₂ production in the water column (bio- and photo-degradation of DOC
593 and POC, plankton metabolism), none seems to be sizably important for persistent CO₂ supersaturation and
594 relevant emissions. The landscape factors of the watershed (bog and forest coverage, soil organic carbon
595 stock) of the tributaries and along the main stem did not sizably affected the C concentration and emission
596 pattern across two seasons. We hypothesize that stable terrestrial input of strongly aromatic DOM, shallow
597 photic layer and humic waters of the Ket River basin preclude sizable daily and seasonal variations of C
598 parameters. Punctual discharge of groundwater, resuspension of sediments or shallow subsurface influx from

599 mires and riparian zone may be responsible for small-scale heterogeneities in C emissions and concentrations
600 along the main stem and among the tributaries. These effects are much stronger pronounced during summer
601 baseflow compared to spring flood. Overall, deeper flow paths in summer compared to spring enhance the
602 DIC discharge within the river bed and the tributaries, thus leading to elevated CO₂ flux in summer.
603 Additional factor responsible for higher CO₂ emission during this season could be mire-originated particulate
604 organic matter (POM) processing in the water column.

605 The six month open-water period C emissions from the lotic waters of the Ket River basin were sizably
606 lower than the downstream total C export by this river during the same period. We conclude that regional
607 estimations of C balance in lotic systems should be based on a combination of direct chamber measurements,
608 discrete hydrochemical sampling and continuous in-situ monitoring with submersible sensors, at least during
609 two most important hydrological periods of the year which are, for boreal regions, the spring flood and the
610 summer-autumn baseflow. We believe that this is the best trade-off between scientific rigor and logistical
611 feasibility in poorly accessible, pristine and strongly understudied regions.

612

613 **Acknowledgements.**

614 We acknowledge support from RSF grant 22-17-00253, RFBR grant 20-05-00729, the TSU Development
615 Program “Priority-2030”, grant “Kolmogorov” of MES (Agreement No 075-15-2022-241), and the Swedish
616 Research Council (grant no. 2016-05275).

617

618 **Authors contribution.**

619 AL and OP designed the study and wrote the paper; AL, SV, IK and OP performed sampling, analysis and
620 their interpretation; LS performed bacterial assessment and DOC/DIC analysis and interpretation; MK
621 performed landscape characterization of the Ket River basin and calculated water surface area; SK
622 performed hydrological analysis; JK provided analyses of literature data, transfer coefficients for FCO₂
623 calculations and global estimations of areal emission vs export.

624

625 **Competing interests.**

626 The authors declare that they have no conflict of interest.

627

628

629 **References**

- 630 Abril, G., Martinez, J.-M., Artigas, L. F., Moreira-Turcq, P., Benedetti, M. F., Vidal, L., Meziane, T., Kim,
631 J.-H., Bernardes, M. C., Savoye, N., Deborde, J., Albéric, P., Souza, M. F. L., Souza, E. L., and Roland,
632 F.: Amazon river carbon dioxide outgassing fueled by wetlands, *Nature*, 505, 395-398,
633 <https://doi.org/10.1038/nature12797>, 2014.
- 634 Abril, G. and Borges, A. V.: Ideas and perspectives: Carbon leaks from flooded land: do we need to replumb
635 the inland water active pipe? *Biogeosciences*, 16, 769–784, <https://doi.org/10.5194/bg-16-769-2019>,
636 2019.
- 637 Ala-Aho, P., Soulsby, C., Pokrovsky, O. S., Kirpotin, S. N., Karlsson, J., Serikova, S., Manasypov, R., Lim,
638 A., Krickov, I., Kolesnichenko, L. G., Laudon, H., and Tetzlaff, D.: Permafrost and lakes control river
639 isotope composition across a boreal Arctic transect in the Western Siberian lowlands, *Environ. Res.
640 Lett.*, 13, <https://doi.org/10.1088/1748-9326/aaa4fe>, 2018a.
- 641 Ala-aho, P., Soulsby, C., Pokrovsky, O. S., Kirpotin, S. N., Karlsson, J., Serikova, S., Vorobyev, S. N.,
642 Manasypov, R. M., Loiko, S., and Tetzlaff, D.: Using stable isotopes to assess surface water source
643 dynamics and hydrological connectivity in a high-latitude wetland and permafrost influenced
644 landscape, *J. Hydrol.*, 556, 279–293, <https://doi.org/10.1016/j.jhydrol.2017.11.024>, 2018b.
- 645 Alin, S. R., Rasera, M. D. F. F. L., Salimon, C. I., Richey, J. E., Holtgrieve, G. W., Krusche, A. V., and
646 Snidvongs, A.: Physical controls on carbon dioxide transfer velocity and flux in low-gradient river
647 systems and implications for regional carbon budgets, *J. Geophys. Res. Biogeosciences*, 116,
648 <https://doi.org/10.1029/2010JG001398>, 2011.
- 649 Allen, G. H. and Pavelsky, T. M.: Global extent of rivers and streams, *Science*, 361, 585–588,
650 <https://doi.org/10.1126/science.aat0636>, 2018.
- 651 Almeida, R. M., Pacheco, F. S., Barros, N., Rosi, E., and Roland, F.: Extreme floods increase CO₂ outgassing
652 from a large Amazonian rive, *Limnol. Oceanogr.*, 62, 989–999, <https://doi.org/10.1002/lno.10480>,
653 2017.
- 654 Amaral, J. H. F., Borges, A. V., Melack, J. M., Sarmiento, H., Barbosa, P. M., Kasper, D., Melo, M. L., de
655 Fex Wolf., D., da Silva, J. S., and Forsberg, B. R.: Influence of plankton metabolism and mixing
656 depth on CO₂ dynamics in an Amazon floodplain lake, *Sci. Total. Env.* 630, 1381-1393,
657 <https://doi.org/10.1016/j.scitotenv.2018.02.331>, 2018.
- 658 Amaral, J. H. F., Melack, J. M., Barbosa, P. M., Borges, A. V., Kasper, D., Cortes, A. C., Zhou, W.,
659 MacIntyre, S., and Forsberg, B. R.: Inundation, hydrodynamics and vegetation influences carbon
660 dioxide concentrations in Amazon floodplain lakes, *Ecosystem*, 25(4), 911–930,
661 <https://doi.org/10.1007/s10021-021-00692-y>, 2022.
- 662 Attermeyer, K., Catalán, N., Einarsdottir, K., Freixa, A., Groeneveld, M., Hawkes, J. A., Bergquist, J., and
663 Tranvik, L. J.: Organic carbon processing during transport through boreal inland waters: particles as
664 important sites, *J. Geophys. Res. Biogeosciences*, 123, 2412–2428,
665 <https://doi.org/10.1029/2018JG004500>, 2018.
- 666 Bartalev, S. A., Egorov, V. A., Ershov, D. V., Isaev, A. S., Lupyan, E. A., Plotnikov, D. E., and Uvarov, I.
667 A.: Remote mapping of vegetation land cover of Russia based on data of MODIS spectroradmeter,
668 *Mod. Probl. Earth Remote Sens. Space*, 8, 285–302, 2018.
- 669 Bastviken, D., Sundgren, I., Natchimuthu, S., Reyier, H., and Gålfalk, M.: Technical Note: Cost-efficient
670 approaches to measure carbon dioxide (CO₂) fluxes and concentrations in terrestrial and aquatic
671 environments using mini loggers, *Biogeosciences*, 12, 3849–3859, [https://doi.org/10.5194/bg-12-3849-](https://doi.org/10.5194/bg-12-3849-2015)
672 2015, 2015.
- 673 Bayer, T. K., Gustafsson, E., Brakebusch, M., and Beer, C.: Future carbon emission from boreal and
674 permafrost lakes are sensitive to catchment organic carbon loads, *J. Geophys. Res. Biogeosciences*,
675 124, 1827-1848, <https://doi.org/10.1029/2018JG004978>, 2019.
- 676 Beaulieu, J. J., Shuster, W. D., and Rebholz, J. A.: Controls on gas transfer velocities in a large river, *J.
677 Geophys. Res. Biogeosciences*, 117, G02007, <https://doi.org/10.1029/2011JG001794>, 2012.
- 678 Borges, A. V., Darchambeau, F., Lambert, T., Bouillon, S., Morana, C., Brouyère, S., Hakoun, V., Jurado,
679 A., Tseng, H-C., Descy, J.-P., and Roland, F. A. E.: Effects of agricultural land use on fluvial carbon

680 dioxide, methane and nitrous oxide concentrations in a large European river, the Meuse (Belgium),
681 *Sci. Total Environ.*, 610-611, 342-355, <https://doi.org/10.1016/j.scitotenv.2017.08.047>, 2018.

682 Borges, A. V., Darchambeau, F., Teodoru, C. R., Marwick, T. R., Tamoooh, F., Geeraert, N., Omengo, F. O.,
683 Guérin, F., Lambert, T., Morana, C., Okuku, E., and Bouillon, S.: Globally significant greenhouse gas
684 emissions from African inland waters, *Nature Geoscience*, 8, 637-642,
685 <https://doi.org/10.1038/NGEO2486>, 2015.

686 Bussmann, I.: Distribution of methane in the Lena Delta and Buor-Khaya Bay, Russia, *Biogeosciences*, 10,
687 4641–4652, <https://doi.org/10.5194/bg-10-4641-2013>, 2013.

688 Cai, W.-J. and Wang, Y.: The chemistry, fluxes, and sources of carbon dioxide in the estuarine waters of the
689 Satilla and Altamaha Rivers, Georgia, *Limnol. Oceanogr.*, 43, 657–668,
690 <https://doi.org/10.4319/lo.1998.43.4.0657>, 1998.

691 Campeau, A. and del Giorgio, P. A.: Patterns in CH₄ and CO₂ concentrations across boreal rivers: Major
692 drivers and implications for fluvial greenhouse emissions under climate change scenarios, *Glob.*
693 *Change Biol.*, 20, 1075–1088, <https://doi.org/10.1111/gcb.12479>, 2014.

694 Campeau, A., Lapierre, J.-F., Vachon, D., and del Giorgio, P. A.: Regional contribution of CO₂ and CH₄
695 fluxes from the fluvial network in a lowland boreal landscape of Québec, *Glob. Biogeochem. Cycles*,
696 28, 57–69, <https://doi.org/10.1002/2013GB004685>, 2014.

697 Castro-Morales, K., Canning, A., Körtzinger, A., Göckede, M., Küsel, K., Overholt, W. A., Wichard, T.,
698 Redlich, S., Arzberger, S., Kolle, O., and Zimov, N.: Effects of reversal of water flow in an Arctic
699 floodplain river on fluvial emissions of CO₂ and CH₄, *J. Geophys. Res. Biogeosciences*, 127,
700 e2021JG006485, <https://doi.org/10.1029/2021JG006485>, 2022.

701 Chadburn, S. E., Krinner, G., Porada, P., Bartsch, A., Beer, C., Beleggi Marchesini, L., Boike, J., Ekici, A.,
702 Elberling, B., Friborg, T., Hugelius, G., Johansson, M., Kuhry, P., Kutzbach, L., Langer, M., Lund, M.,
703 Parmentier, F.-J. W., Peng, S., Van Huissteden, K., Wang, T., Westermann, S., Zhu, D., and Burke, E.
704 J.: Carbon stocks and fluxes in the high latitudes: using site-level data to evaluate Earth system models,
705 *Biogeosciences*, 14, 5143–5169, <https://doi.org/10.5194/bg-14-5143-2017>, 2017.

706 Cole, J. J. and Caraco, N. F.: Atmospheric exchange of carbon dioxide in a low-wind oligotrophic lake
707 measured by the addition of SF₆, *Limnol. Oceanogr.*, 43, 647–656,
708 <https://doi.org/10.4319/lo.1998.43.4.0647>, 1998.

709 Cooper, L. W., McClelland, J. W., Holmes, R. M., Raymond, P. A., Gibson, J. J., Guay, C. K., and Peterson,
710 B. J.: Flow-weighted values of runoff tracers ($\delta^{18}\text{O}$, DOC, Ba, alkalinity) from the six largest Arctic
711 rivers, *Geophys. Res. Lett.*, 35, L18606, <https://doi.org/10.1029/2008GL035007>, 2008.

712 Crawford, J. T., Striegl, R. G., Wickland, K. P., Dornblaser, M. M., and Stanley, E. H.: Emissions of carbon
713 dioxide and methane from a headwater stream network of interior Alaska, *J. Geophys. Res.*
714 *Biogeosciences*, 118, 482–494, <https://doi.org/10.1002/jgrg.20034>, 2013.

715 Crawford, J. T., Loken, L. C., Casson, N. J., Smith, C., Stone, A. G., and Winslow, L. A.: High-speed
716 limnology: using advanced sensors to investigate spatial variability in biogeochemistry and hydrology,
717 *Environ. Sci. Technol.*, 49, 442–450, <https://doi.org/10.1021/es504773x>, 2015.

718 Crawford, J. T., Stanley, E. H., Dornblaser, M. M., and Striegl, R. G.: CO₂ time series patterns in
719 contrasting headwater streams of North America, *Aquatic Sciences*, 79, 473-
720 486, <https://doi.org/10.1007/s00027-016-0511-2>, 2016a.

721 Crawford, J. T., Loken, L. C., Stanley, E. H., Stets, E. G., Dornblaser, M. M., and Striegl, R. G.: Basin scale
722 controls on CO₂ and CH₄ emissions from the Upper Mississippi River, *Geophys. Res. Lett.*, 43, 1973–
723 1979, <https://doi.org/10.1002/2015GL067599>, 2016b.

724 Crawford, J. T., Butman, D. E., Loken, L. C., Stadler, P., Kuhn, C., and Striegl, R. G.: Spatial variability of
725 CO₂ concentrations and biogeochemistry in the Lower Columbia River, *Inland Waters*, 7, 417-427,
726 <https://doi.org/10.1080/20442041.2017.1366487>, 2017.

727 Dawson, J. J., Billett, M. F., Hope, D., Palmer, S. M., and Deacon, C.: Sources and sinks of aquatic carbon
728 in a peatland stream continuum, *Biogeochemistry*, 70, 71–92, 2004.

729 Descy, J. P., Darchambeau, F., Lambert, T., Stoyneva, M. P., Bouillon, S., and Borges, A. V.: Phytoplankton
730 dynamics in the Congo River, *Freshwater Biology*, 62, 87–101, <https://doi.org/10.1111/fwb.12851>,
731 2017.

732 DelDuco, E. M. and Xu, Y. J.: Dissolved carbon transport and processing in North America's largest swamp
733 river entering the Northern Gulf of Mexico, *Water*, 11, 1395, <https://doi.org/10.3390/w11071395>, 2019.

734 Denfeld, B. A., Frey, K. E., Sobczak, W. V., Mann, P. J., and Holmes, R. M.: Summer CO₂ evasion from
735 streams and rivers in the Kolyma River basin, north-east Siberia, *Polar Res.*, 32, 19704,
736 <https://doi.org/10.3402/polar.v32i0.19704>, 2013.

737 Dinsmore, K. J. and Billett, M. F.: Continuous measurement and modeling of CO₂ losses from a peatland
738 stream during stormflow events, *Water Resour. Res.*, 44, W12417,
739 <https://doi.org/10.1029/2008WR007284>, 2008.

740 Dinsmore, K. J., Billett, M. F., and Dyson, K. E.: Temperature and precipitation drive temporal variability in
741 aquatic carbon and GHG concentrations and fluxes in a peatland catchment, *Glob. Change Biol.*, 19,
742 2133–2148, <https://doi.org/10.1111/gcb.12209>, 2013.

743 Elder, C. D., and others.: Greenhouse gas emissions from diverse Arctic Alaskan lakes are dominated by
744 young carbon, *Nature Climate Change* 8, 166–171, doi: 10.1038/s41558-017-0066-9, 2018.

745 Feng, X., Vonk, J. E., Dongen, B. E. V., Gustafsson, Ö., Semiletov, I. P., Dudarev, O. V., Wang, Z.,
746 Montluçon, D. B., Wacker, L., and Eglinton, T. I.: Differential mobilization of terrestrial carbon pools
747 in Eurasian Arctic river basins, *Proc. Natl. Acad. Sci. U. S. A.*, 110, 14168–14173,
748 <https://doi.org/10.1073/pnas.1307031110>, 2013.

749 Foster-Martinez, M. R. and Variano, E. A.: Air-water gas exchange by waving vegetation stems, *J. Geophys.*
750 *Res. Biogeosciences*, 121, 1916–1923, <https://doi.org/10.1002/2016JG003366>, 2016.

751 Frey, K. E. and Smith, L. C.: How well do we know northern land cover? Comparison of four global
752 vegetation and wetland products with a new ground-truth database for West Siberia. *Glob. Biogeochem.*
753 *Cycles*, 21, GB1016. <https://doi.org/10.1029/2006GB002706>, 2007.

754 Frey, K. E. and McClelland, J. W.: Impacts of permafrost degradation on arctic river biogeochemistry,
755 *Hydrol. Process.*, 23, 169–182, <https://doi.org/10.1002/hyp.7196>, 2009.

756 Gómez-Gener, L., Rocher-Ros, G., Battin, T., Cohen, M. J., Dalmagro, H. J., Dinsmore, K. J., Drake, T. W.,
757 Duvert, C., Enrich-Prast, A., Horgby, Å., Johnson, M. S., Kirk, L., Machado-Silva, F., Marzolf, N. S.,
758 McDowell, M. J., McDowell, W. H., Miettinen, H., Ojala, A. K., Peter, H., Pumpanen, J., Ran, L.,
759 Riveros-Iregui, D. A., Santos, I. R., Six, J., Stanley, E. H., Wallin, M. B., White, S. A., and Sponseller,
760 R. A.: Global carbon dioxide efflux from rivers enhanced by high nocturnal emissions, *Nat. Geosci.*,
761 1–6, <https://doi.org/10.1038/s41561-021-00722-3>, 2021a.

762 Gómez-Gener, L., Hotchkiss, E. R., Laudon, H., and Sponseller, R. A.: Integrating discharge-concentration
763 dynamics across carbon forms in a boreal landscape, *Water Resour. Res.*, 57, e2020WR028806,
764 <https://doi.org/10.1029/2020WR028806>, 2021b.

765 Griffin, C. G., McClelland, J. W., Frey, K. E., Fiske, G., and Holmes, R. M.: Quantifying CDOM and DOC
766 in major Arctic rivers during ice-free conditions using Landsat TM and ETM+ data, *Remote Sens.*
767 *Environ.*, 209, 395–409, <https://doi.org/10.1016/j.rse.2018.02.060>, 2018.

768 Guérin, F., Abril, G., Serça, D., Delon, C., Richard, S., Delmas, R., Tremblay, A., and Varfalvy, L.: Gas
769 transfer velocities of CO₂ and CH₄ in a tropical reservoir and its river downstream, *J. Mar. Syst.*, 66,
770 161–172, <https://doi.org/10.1016/j.jmarsys.2006.03.019>, 2007.

771 Harris, I., Jones, P. d., Osborn, T. j., and Lister, D. h.: Updated high-resolution grids of monthly climatic
772 observations – the CRU TS3.10 Dataset, *Int. J. Climatol.*, 34, 623–642,
773 <https://doi.org/10.1002/joc.3711>, 2014.

774 Ho, D. T., Engel, V. C., Ferrón, S., Hickman, B., Choi, J., and Harvey, J. W.: On factors influencing air-water
775 gas exchange in emergent wetlands, *J. Geophys. Res. Biogeosciences*, 123, 178–192,
776 <https://doi.org/10.1002/2017JG004299>, 2018.

777 Holmes, R. M., McClelland, J. W., Peterson, B.J., & Tank S. E. et al. Seasonal and annual fluxes of nutrients
778 and organic matter from large rivers to the Arctic Ocean and surrounding seas, *Estuaries and Coasts*,
779 35, 369–382. doi: 10.1007/s12237-011-9386-6, 2012.

780 Holmes, R. M., Coe, M. T., Fiske, G. J., Gurtovaya, T., McClelland, J. W., Shiklomanov, A. I., Spencer, R.
781 G. M., Tank, S. E., and Zhulidov, A. V.: Climate change impacts on the hydrology and biogeochemistry
782 of Arctic Rivers, in: *Climatic Changes and Global warming of Inland Waters: Impacts and Mitigation*
783 *for Ecosystems and Societies*, edited by: Goldman, C. R., Kumagi, M., and Robarts, R. D., John Wiley
784 and Sons, 1–26, 2013.

785 Hotchkiss, E. R., Hall Jr, R. O., Sponseller, R. A., Butman, D., Klaminder, J., Laudon, H., Rosvall, M., and
786 Karlsson, J.: Sources of and processes controlling CO₂ emissions change with the size of streams and
787 rivers, *Nat. Geosci.*, 8, 696–699, <https://doi.org/10.1038/ngeo2507>, 2015.

788 Hugelius, G., Tarnocai, C., Broll, G., Canadell, J. G., Kuhry, P., and Swanson, D. K.: The northern
789 circumpolar soil carbon database: Spatially distributed datasets of soil coverage and soil carbon storage
790 in the northern permafrost regions, *Earth Syst. Sci. Data*, 5, 3–13, [https://doi.org/10.5194/essd-5-3-](https://doi.org/10.5194/essd-5-3-2013)
791 2013, 2013.

792 Humborg, C., Mörth, C.-M., Sundbom, M., Borg, H., Blenckner, T., Giesler, R., and Ittekkot, V.: CO₂
793 supersaturation along the aquatic conduit in Swedish watersheds as constrained by terrestrial
794 respiration, aquatic respiration and weathering, *Glob. Change Biol.*, 16, 1966–1978,
795 <https://doi.org/10.1111/j.1365-2486.2009.02092.x>, 2010.

796 Hutchins, R. H. S., Prairie, Y. T., and del Giorgio, P. A.: Large-Scale Landscape Drivers of CO₂, CH₄, DOC,
797 and DIC in Boreal River Networks, *Glob. Biogeochem. Cycles*, 33, 125–142,
798 <https://doi.org/10.1029/2018GB006106>, 2019.

799 Hutchins, R. H. S., Tank, S. E., Olefeldt, D., Quinton, W. L., Spence, C., Dion, N., Estop-Aragonés, C., and
800 Mengistu, S. G.: Fluvial CO₂ and CH₄ patterns across wildfire-disturbed ecozones of subarctic Canada:
801 Current status and implications for future change, *Glob. Change Biol.*, 26, 2304–2319,
802 <https://doi.org/10.1111/gcb.14960>, 2020.

803 Johnson, M. S., Billett, M. F., Dinsmore, K. J., Wallin, M., Dyson, K. E., and Jassal, R. S.: Direct and
804 continuous measurement of dissolved carbon dioxide in freshwater aquatic systems—method and
805 applications, *Ecohydrology*, 3, 68–78, <https://doi.org/10.1002/eco.95>, 2009.

806 Jonsson, A., Algesten, G., Bergström, A.-K., Bishop, K., Sobek, S., Tranvik, L. J., and Jansson, M.:
807 Integrating aquatic carbon fluxes in a boreal catchment carbon budget, *J. Hydrol.*, 334, 141–150,
808 <https://doi.org/10.1016/j.jhydrol.2006.10.003>, 2007.

809 Karlsson, J., Serikova, S., Vorobyev, S. N., Rocher-Ros, G., Denfeld, B., and Pokrovsky, O. S.: Carbon
810 emission from Western Siberian inland waters, *Nat. Commun.*, 12, 825, [https://doi.org/10.1038/s41467-](https://doi.org/10.1038/s41467-021-21054-1)
811 021-21054-1, 2021.

812 Kokic, J., Wallin, M. B., Chmiel, H. E., Denfeld, B. A., and Sobek, S.: Carbon dioxide evasion from
813 headwater systems strongly contributes to the total export of carbon from a small boreal lake catchment,
814 *J. Geophys. Res. Biogeosciences*, 120, 13–28, <https://doi.org/10.1002/2014JG002706>, 2015.

815 Koprivnjak, J.-F., Dillon, P. J., and Molot, L. A.: Importance of CO₂ evasion from small boreal streams, *Glob.*
816 *Biogeochem. Cycles*, 24, GB4003, <https://doi.org/10.1029/2009GB003723>, 2010.

817 Krickov, I. V., Lim, A. G., Manasypov, R. M., Loiko, S. V., Shirokova, L. S., Kirpotin, S. N., Karlsson, J.,
818 and Pokrovsky, O. S.: Riverine particulate C and N generated at the permafrost thaw front: Case study
819 of western Siberian rivers across a 1700 km latitudinal transect, *Biogeosciences*, 6867–6884,
820 <https://doi.org/10.5194/bg-15-6867-2018>, 2018.

821 Krickov, I. V., Serikova, S., Pokrovsky, O. S., Vorobyev, S. N., Lim, A. G., Siewert, M. B., and Karlsson, J.:
822 Sizable carbon emission from the floodplain of Ob River, *Ecol. Indic.*, 131, 108164,
823 <https://doi.org/10.1016/j.ecolind.2021.108164>, 2021.

824 Lauerwald, R., Laruelle, G. G., Hartmann, J., Ciais, P., and Regnier, P. A. G.: Spatial patterns in CO₂ evasion
825 from the global river network, *Glob. Biogeochem. Cycles*, 29, 534–554,
826 <https://doi.org/10.1002/2014GB004941>, 2015.

827 Laurion, I., Vincent, W. F., MacIntyre, S., Retamal, L., Dupont, C., Francus, P., and Pienitz, R.: Variability
828 in greenhouse gas emissions from permafrost thaw ponds, *Limnol. Oceanogr.*, 55, 115–133,
829 <https://doi.org/10.4319/lo.2010.55.1.0115>, 2010.

830 Leith, F. I., Dinsmore, K. J., Wallin, M. B., Billett, M. F., Heal, K. V., Laudon, H., Öquist, M. G., and Bishop,
831 K.: Carbon dioxide transport across the hillslope–riparian–stream continuum in a boreal headwater
832 catchment, *Biogeosciences*, 12, 1881–1892, <https://doi.org/10.5194/bg-12-1881-2015>, 2015.

833 Leng, P., Li, Z., Zhang, Q., Li, F., and Koschorreck, M.: Fluvial CO₂ and CH₄ in a lowland agriculturally
834 impacted river network: Importance of local and longitudinal controls, *Environ. Pollution* 303, Art No
835 119125, <https://doi.org/10.1016/j.envpol.2022.119125>, 2022.

836 Li, M., Peng, C., Zhang, K., Xu, L., Wang, J., Yang, Y., Li, P., Liu, Z., and He, N.: Headwater stream
837 ecosystem: an important source of greenhouse gases to the atmosphere, *Water Res.*, 190, 116738,
838 <https://doi.org/10.1016/j.watres.2020.116738>, 2021.

839 Liss, P. S., and Slater, P. G.: Flux of gases across the air-sea interface, *Nature* 247, 181–184, 1974.

840 Liu S., Kuhn, C., Amatulli, G., Aho, K., Butman, D.E., Allen, G.H., Lin, P., Pan, M., Yamazaki, D.,
841 Brinkerhoff, C., Gleason, C., Xia, X., and Raymond, P.A.: The importance of hydrology in routing
842 terrestrial carbon to the atmosphere via global streams and rivers, *PNAS* 119 No. 11, e2106322119;
843 <https://doi.org/10.1073/pnas.2106322119>, 2022.

844 Lobbes, J. M., Fitznar, H. P., and Kattner, G.: Biogeochemical characteristics of dissolved and particulate
845 organic matter in Russian rivers entering the Arctic Ocean, *Geochim. Cosmochim. Acta*, 64, 2973–
846 2983, [https://doi.org/10.1016/S0016-7037\(00\)00409-9](https://doi.org/10.1016/S0016-7037(00)00409-9), 2000.

847 Lorke A., Bodmer, P., Noss, C., Alshboul, Z., Koschorreck, M., Somlai-Haase, C., Bastviken, D., Flury, S.,
848 McGinnis, D.F., Maeck, A., Müller, D., and Premke, K.: Technical note: drifting versus anchored
849 flux chambers for measuring greenhouse gas emissions from running waters, *Biogeosciences*, 12,
850 7013–7024, <https://doi.org/10.5194/bg-12-7013-2015>, 2015.

851 Lundin, E. J., Giesler, R., Persson, A., Thompson, M. S., and Karlsson, J.: Integrating carbon emissions from
852 lakes and streams in a subarctic catchment, *J. Geophys. Res. Biogeosciences*, 118, 1200–1207,
853 <https://doi.org/10.1002/jgrg.20092>, 2013.

854 Lynch, L. M., Sutfin, N. A., Fegcl, T. S., Boot, C. M., Covino, T. P., and Wallenstein, M. D.: River channel
855 connectivity shifts metabolite composition and dissolved organic matter chemistry, *Nat. Commun.*, 10,
856 459, <https://doi.org/10.1038/s41467-019-08406-8>, 2019.

857 Marie, D., Partensky, F., Vaulot, D., and Brussaard, C.: Enumeration of Phytoplankton, Bacteria, and Viruses
858 in Marine Samples, *Curr. Protoc. Cytom.*, 10, 11111–111115,
859 <https://doi.org/10.1002/0471142956.cy1111s10>, 1999.

860 Pangala, S., Enrich-Prast, A., Basso, L., Peixoto, R. B., Bastviken, D., Hornibrook, E. R. C., Gatti, L. V.,
861 Ribeiro, H., et al.: Large emissions from floodplain trees close the Amazon methane budget, *Nature*
862 552, 230–234, <https://doi.org/10.1038/nature24639>, 2017.

863 Pekel, J.-F., Cottam, A., Gorelick, N., and Belward, A. S.: High-resolution mapping of global surface water
864 and its long-term changes, *Nature*, 540, 418–422, <https://doi.org/10.1038/nature20584>, 2016.

865 Pokrovsky, O. S., Manasypov, R. M., Loiko, S., Shirokova, L. S., Krickov, I. A., Pokrovsky, B. G.,
866 Kolesnichenko, L. G., Kopysov, S. G., Zemtsov, V. A., Kulizhsky, S. P., Vorobyev, S. N., and Kirpotin,
867 S. N.: Permafrost coverage, watershed area and season control of dissolved carbon and major elements
868 in western Siberian rivers, *Biogeosciences*, 12, 6301–6320, <https://doi.org/10.5194/bg-12-6301-2015>,
869 2015.

870 Pokrovsky, O. S., Manasypov, R. M., Kopysov, S. G., Krickov, I. V., Shirokova, L. S., Loiko, S. V., Lim, A.
871 G., Kolesnichenko, L. G., Vorobyev, S. N., and Kirpotin, S. N.: Impact of permafrost thaw and climate
872 warming on riverine export fluxes of carbon, nutrients and metals in Western Siberia, *Water (MDPI)*,
873 12, 1817, <https://doi.org/10.3390/w12061817>, 2020.

874 Pokrovsky, O. S., Manasypov, R. M., Chupakov, A. V., and Kopysov, S.: Element transport in the Taz River,
875 western Siberia, *Chemical Geology*, in press, 2022.

876 Ran, L., Lu, X. X., Richey, J. E., Sun, H., Han, J., Yu, R., Liao, S., and Yi, Q.: Long-term spatial and temporal
877 variation of CO₂ partial pressure in the Yellow River, China, *Biogeosciences*, 12, 921–932,
878 <https://doi.org/10.5194/bg-12-921-2015>, 2015.

879 Ran, L., Lu, X. X., and Liu, S.: Dynamics of riverine CO₂ in the Yangtze River fluvial network and their
880 implications for carbon evasion, *Biogeosciences*, 14, 2183–2198, <https://doi.org/10.5194/bg-14-2183-2017>,
881 2017.

882 Raymond, P. A., McClelland, J. W., Holmes, R. M., Zhulidov, A. V., Mull, K., Peterson, B. J., Striegl, R. G.,
883 Aiken, G. R., and Gurtovaya, T. Y.: Flux and age of dissolved organic carbon exported to the Arctic
884 Ocean: A carbon isotopic study of the five largest arctic rivers, *Glob. Biogeochem. Cycles*, 21, GB4011,
885 <https://doi.org/10.1029/2007GB002934>, 2007.

886 Raymond, P. A., Hartmann, J., Lauerwald, R., Sobek, S., McDonald, C., Hoover, M., Butman, D., Striegl,
887 R., Mayorga, E., Humborg, C., Kortelainen, P., Dürr, H., Meybeck, M., Ciais, P., and Guth, P.: Global

888 carbon dioxide emissions from inland waters, *Nature*, 503, 355–359,
889 <https://doi.org/10.1038/nature12760>, 2013.

890 Repo, M. E., Huttunen, J. T., Naumov, A. V., Chichulin, A. V., Lapshina, E. D., Bleuten, W., and
891 Martikainen, P. J.: Release of CO₂ and CH₄ from small wetland lakes in western Siberia, *Tellus Ser.*
892 *B, Chem. Phys. Meteorol.*, 59, 788–796. doi: 10.1111/j.1600-0889.2007.00301.x, 2007.

893 Rocher-Ros, G., Sponseller, R. A., Lidberg, W., Mörth, C.-M., and Giesler, R.: Landscape process domains
894 drive patterns of CO₂ evasion from river networks, *Limnol. Oceanogr. Lett.*, 4, 87–95,
895 <https://doi.org/10.1002/lol2.10108>, 2019.

896 Santoro, M., Beer, C., Cartus, O., Schmullius, C., Shvidenko, A., McCallum, I., Wegmüller, U., and
897 Wiesmann, A.: The BIOMASAR algorithm: An approach for retrieval of forest growing stock volume
898 using stacks of multi-temporal SAR data, in: *Proceedings of ESA Living Planet Symposium*, Bergen,
899 Norway, 28 June – 2 July, 2010.

900 Schneider, C. L., Herrera, M., Raisle, M. L., Suarez, E., and Riveros-Iregui, D. A.: Carbon Dioxide (CO₂)
901 Fluxes from terrestrial and aquatic environments in a high altitude tropical catchment. *J Geophys.*
902 *Res. Biogeosciences* 125, e2020JG005844. <https://doi.org/10.1029/2020JG005844>, 2020.

903 Semiletov, I. P., Pipko, I. I., Shakhova, N. E., Dudarev, O. V., Pugach, S. P., Charkin, A. N., McRoy, C. P.,
904 Kosmach, D., and Gustafsson, Ö.: Carbon transport by the Lena River from its headwaters to the Arctic
905 Ocean, with emphasis on fluvial input of terrestrial particulate organic carbon vs. carbon transport by
906 coastal erosion, *Biogeosciences*, 8, 2407–2426, <https://doi.org/10.5194/bg-8-2407-2011>, 2011.

907 Serikova, S., Pokrovsky, O. S., Ala-Aho, P., Kazantsev, V., Kirpotin, S. N., Kopysov, S. G., Krickov, I. V.,
908 Laudon, H., Manasypov, R. M., Shirokova, L. S., Soulsby, C., Tetzlaff, D., and Karlsson, J.: High
909 riverine CO₂ emissions at the permafrost boundary of Western Siberia, *Nat. Geosci.*, 11, 825–829,
910 <https://doi.org/10.1038/s41561-018-0218-1>, 2018.

911 Serikova, S., Pokrovsky, O. S., Laudon, H., Krickov, I. V., Lim, A. G., Manasypov, R. M., and Karlsson, J.:
912 High carbon emissions from thermokarst lakes of Western Siberia, *Nat. Commun.*, 10,
913 <https://doi.org/10.1038/s41467-019-09592-1>, 2019.

914 Stackpoole, S. M., Butman, D. E., Clow, D. W., Verdin, K. L., Gaglioti, B. V., Genet, H., and Striegl, R. G.:
915 Inland waters and their role in the carbon cycle of Alaska, *Ecol. Appl.*, 27, 1403–1420,
916 <https://doi.org/10.1002/eap.1552>, 2017.

917 Striegl, R. G., Dornblaser, M. M., McDonald, C. P., Rover, J. A., and Stets, E. G.: Carbon dioxide and
918 methane emissions from the Yukon River system, *Glob. Biogeochem. Cycles*, 26, GB0E05,
919 <https://doi.org/10.1029/2012GB004306>, 2012.

920 Teodoru, C. R., del Giorgio, P. A., Prairie, Y. T., and Camire, M.: Patterns in pCO₂ in boreal streams and
921 rivers of northern Quebec, Canada, *Glob. Biogeochem. Cycles*, 23, GB2012,
922 <https://doi.org/10.1029/2008GB003404>, 2009.

923 Tranvik, L., Cole, J. J., and Prairie, Y. T.: The study of carbon in inland waters-from isolated ecosystems to
924 players in the global carbon cycle, *Limnol. Oceanogr. Lett.*, 3, 41–48,
925 <https://doi.org/10.1002/lol2.10068>, 2018.

926 Turetsky, M.R., Abbott, B.W., Jones, M.C., Anthony, K.W., Olefeldt, D., Schuur, E.A.G., Grosse, G., Kuhry,
927 P., Hugelius, G., Koven, C., et al. : Carbon release through abrupt permafrost thaw, *Nat. Geoscience*,
928 13, 138–143, doi:10.1038/s41561-019-0526-0, 2020.

929 Vachon, D., Sponseller, R. A., and Karlsson, J.: Integrating carbon emission, accumulation and transport in
930 inland waters to understand their role in the global carbon cycle, *Glob. Change Biol.*, 27, 719–727,
931 <https://doi.org/10.1111/gcb.15448>, 2021.

932 Vorobyev, S. N., Pokrovsky, O. S., Kolesnichenko, L. G., Manasypov, R. M., Shirokova, L. S., Karlsson, J.,
933 and Kirpotin, S. N.: Biogeochemistry of dissolved carbon, major, and trace elements during spring flood
934 periods on the Ob River, *Hydrol. Process.*, 33, 1579–1594, <https://doi.org/10.1002/hyp.13424>, 2019.

935 Vorobyev, S. N., Karlsson, J., Kolesnichenko, Y. Y., Korets, M. A., and Pokrovsky, O. S.: Fluvial carbon
936 dioxide emission from the Lena River basin during the spring flood, *Biogeosciences*, 18, 4919–4936,
937 <https://doi.org/10.5194/bg-18-4919-2021>, 2021.

938 Wallin, M. B., Öquist, M. G., Buffam, I., Billett, M. F., Nisell, J., and Bishop, K. H.: Spatiotemporal
939 variability of the gas transfer coefficient (KCO₂) in boreal streams: Implications for large scale

940 estimates of CO₂ evasion, *Glob. Biogeochem. Cycles*, 25, GB3025,
941 <https://doi.org/10.1029/2010GB003975>, 2011.

942 Wallin, M. B., Grabs, T., Buffam, I., Laudon, H., Ågren, A., Öquist, M. G., and Bishop, K.: Evasion of CO₂
943 from streams – The dominant component of the carbon export through the aquatic conduit in a boreal
944 landscape, *Glob. Change Biol.*, 19, 785–797, <https://doi.org/10.1111/gcb.12083>, 2013.

945 Wallin, M. B., Campeau, A., Audet, J., Bastviken, D., Bishop, K., Kokic, J., Laudon, H., Lundin, E., Löfgren,
946 S., Natchimuthu, S., Sobek, S., Teutschbein, C., Weyhenmeyer, G. A., and Grabs, T.: Carbon dioxide
947 and methane emissions of Swedish low-order streams—a national estimate and lessons learnt from
948 more than a decade of observations, *Limnol. Oceanogr. Lett.*, 3, 156–167,
949 <https://doi.org/10.1002/lol2.10061>, 2018.

950 Wanninkhof, R.: Relationship between wind speed and gas exchange over the ocean, *J. Geophys. Res.*
951 *Oceans*, 97, 7373–7382, <https://doi.org/10.1029/92JC00188>, 1992.

952 Wild, B., Andersson, A., Bröder, L., Vonk, J., Hugelius, G., McClelland, J. W., Song, W., Raymond, P. A.,
953 and Gustafsson, Ö.: Rivers across the Siberian Arctic unearth the patterns of carbon release from
954 thawing permafrost, *PNAS*, 116, 10280–10285, <https://doi.org/10.1073/pnas.1811797116>, 2019.

955 Winterdahl, M., Wallin, M. B., Karlsen, R. H., Laudon, H., Öquist, M., and Lyon, S. W.: Decoupling of
956 carbon dioxide and dissolved organic carbon in boreal headwater streams, *J. Geophys. Res.*
957 *Biogeosciences*, 121, 2630–2651, <https://doi.org/10.1002/2016JG003420>, 2016.

958 Yamamoto, S., Alcauskas, J. B., and Crozier, T. E.: Solubility of methane in distilled water and seawater. *J.*
959 *Chem. Eng. Data*. 21, 78–80, 1976.

960 Zabelina, S. V., Shirokova, L. S., Klimov, S I., Chupakov, A. V., Lim, A. G., Polishchuk, Y. M., Polishchuk,
961 V. M., Bogdanov, A. N., Muratov, I. N., Gueren, F., Karlsson, J., and Pokrovsky, O. S.: Seasonal and
962 spatial variations of CO₂ and CH₄ concentrations and fluxes in surface waters of frozen peatlands (NE
963 Europe): morphological and hydrochemical control, *Limnology Oceanography*, 66 (S1), S216-S230,
964 doi: 10.1002/lno.11560, 2021.

965 Zolkos, S., Tank, S. E., Striegl, R. G., and Kokelj, S. V.: Thermokarst effects on carbon dioxide and methane
966 fluxes in streams on the Peel Plateau (NWT, Canada), *J. Geophys. Res. Biogeosciences*, 124, 1781–
967 1798, <https://doi.org/10.1029/2019JG005038>, 2019.

968

969

970

971

972

973

974

975

976

977

978

979

980

981

982

983

984

985

986 **Table 1.** Measured hydrochemical and GHG exchange parameters in the Ket River main stem and
 987 tributaries (average \pm s.d.; (*n*) is number of measurements).

988

989

Parameter	unit	Tributaries		Main stem	
		Flood (<i>n</i> =26)	Base flow (<i>n</i> =12)	Flood (<i>n</i> =7)	Base flow (<i>n</i> =6)
Water temperature	°C	9.48 \pm 2.25	14.9 \pm 1.24	9.06 \pm 1.59	16.5 \pm 0.54
pH		6.31 \pm 0.45	6.71 \pm 0.57	6.2 \pm 0.43	7.29 \pm 0.26
Dissolved O ₂	mg L ⁻¹	8.53 \pm 1.26	8.02 \pm 1.13	8.85 \pm 0.83	8.78 \pm 0.18
Specific Conductivity	μS cm ⁻¹	40.7 \pm 22.7	126.9 \pm 62.1	39 \pm 14.9	181 \pm 36.8
DIC	mg L ⁻¹	2.83 \pm 2.58	17.8 \pm 10.4	2.43 \pm 1.49	20.5 \pm 5.22
DOC	mg L ⁻¹	21.7 \pm 3.94	15.7 \pm 7.04	21.9 \pm 4.28	16.6 \pm 3.57
SUVA ₂₅₄	L mg C ⁻¹ m ⁻¹	4.34 \pm 0.33	4.9 \pm 0.66	4.29 \pm 0.18	4.26 \pm 0.52
PON	mg L ⁻¹	0.08 \pm 0.06	0.64 \pm 0.27	0.1 \pm 0.07	0.96 \pm 0.22
POC	mg L ⁻¹	2.41 \pm 1.17	8 \pm 2.36	2.55 \pm 1.2	9.49 \pm 1.98
TBC	*10 ⁵ cells ml ⁻¹	5.89 \pm 3.26	8.69 \pm 3.21	5.95 \pm 2.83	4.94 \pm 2.15
K _T	m d ⁻¹	0.53 \pm 0.38	1.21 \pm 0.52	0.77 \pm 0.55	1.22 \pm 0.37
FCO ₂	g C m ⁻² d ⁻¹	1.3 \pm 0.76	2.63 \pm 2.15	1.35 \pm 1.08	1.16 \pm 0.5
pCO ₂	μatm	2880 \pm 680	4000 \pm 1500	2400 \pm 330	2520 \pm 980
FCH ₄	mmol C m ⁻² d ⁻¹	0.39 \pm 0.95	1.38 \pm 1.21	0.06 \pm 0.05	0.95 \pm 0.88
CH ₄	μmol L ⁻¹	0.65 \pm 0.66	1.17 \pm 0.81	0.17 \pm 0.01	0.86 \pm 0.91

990

991

992

993

994

995

996

997

998

999

1000

1001

1002

1003

1004

1005

1006

1007

1008

1009

1010

1011

1012

1013

1014

1015

1016

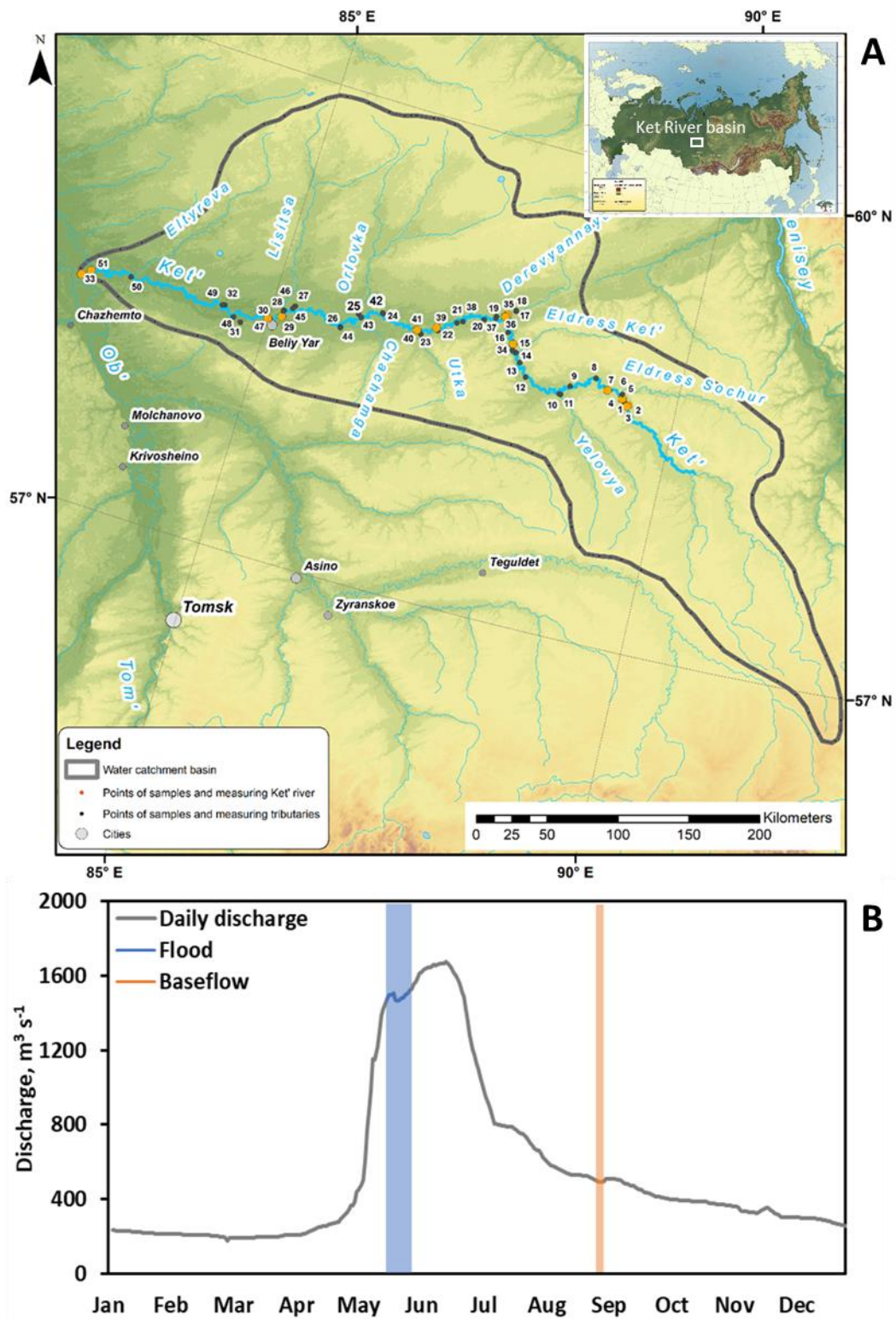
1017

1018
 1019
 1020
 1021
 1022
 1023

Table 2. Pearson correlation coefficients of measured FCO₂, CO₂, and CH₄ concentration with hydrochemical parameters of the water column (DOC, SUVA, particulate organic carbon and nitrogen, total bacterial cells) and landscape parameters of the tributaries and the main stem of the Ket River. Significant (p < 0.05) values are labeled by asterisk.

	all seasons			flood			baseflow		
	CH ₄	CO ₂	FCO ₂	CH ₄	CO ₂	FCO ₂	CH ₄	CO ₂	FCO ₂
Hydrochemical parameters									
pH	0.2	-0.1	-0.2	-0.1	0.1	-0.2	0.0	-0.6*	-0.6*
Dissolved O ₂	-0.1	-0.7*	-0.1	0.0	-0.8*	0.1	-0.2	-0.8*	-0.7*
Specific conductivity	0.3	0.0	0.1	-0.2	0.0	0.1	0.2	-0.3	-0.6*
DIC	0.3	0.0	0.0	-0.1	0.0	0.1	0.2	-0.4	-0.7*
DOC	-0.1	0.0	0.1	0.3	0.0	-0.1	-0.2	-0.1	0.2
SUVA ₂₅₄	0.1	0.2	0.3	0.4	-0.3	0.1	-0.2	0.5*	0.6*
PON	0.1	-0.1	0.2	-0.2	-0.4*	0.2	-0.4	-0.5*	-0.5
POC	0.1	-0.1	0.2	-0.2	-0.4*	0.1	-0.3	-0.3	0.1
TBC	0.2	0.2	0.1	0.3	-0.2	-0.1	0.0	0.5*	0.5*
Climatic characteristics									
MAAT	0.2	0.0	-0.5*	0.1	0.0	-0.4*	0.2	0.1	-0.5
MAP	0.0	0.3*	0.5*	0.1	0.0	0.3	0.1	0.6*	0.7*
Land-cover characteristics									
Watershed area	-0.3	-0.3*	0.2	-0.4	-0.5*	0.0	-0.2	-0.1	0.5
Dark Needleleaf Forest	0.1	0.0	-0.3	0.1	0.0	-0.3	0.2	-0.1	-0.2
Light Needleleaf Forest	0.3*	0.4*	0.2	0.4	0.2	0.0	0.4	0.7*	0.6*
Broadleaf Forest	-0.3	-0.4*	0.1	-0.5*	-0.4	0.1	-0.3	-0.6*	-0.2
Mixed Forest	0.0	-0.2	-0.3	0.1	-0.1	-0.3	-0.1	-0.4	-0.4
Peatlands and bogs	0.0	0.2	0.3	-0.1	0.0	0.2	0.1	0.2	0.4
Riparian Vegetation	-0.1	0.0	-0.1	-0.2	0.1	0.0	-0.2	-0.2	-0.5
Grassland	0.1	-0.1	0.0	-0.1	-0.2	0.1	0.3	0.0	-0.5
Recent Burns	-0.1	-0.1	0.2	-0.1	-0.2	0.1	-0.3	0.1	0.4
Water Bodies	-0.2	-0.1	0.3	-0.3	-0.3	0.2	-0.2	-0.1	0.3
Lithology characteristics									
Upper Cretaceous, Maastrichtian – (sedimentary, silicate)	0.1	-0.4*	0.0	0.3	-0.3	0.2	0.0	-0.5*	-0.4
Lower Paleocene (sedimentary silicate rocks)									
Paleogene. Upper Oligocene (clays and silts)	0.1	-0.2	0.1	0.1	-0.1	0.2	0.0	-0.5*	-0.2
Cretaceous. Coniacian – Campanian (carbonates)	-0.2	-0.4*	-0.3	-0.2	-0.2	-0.2	-0.3	-0.7*	-0.6*
Cretaceous. Cenoman – Turon (clays, some carbonates)	-0.2	-0.5*	-0.3	-0.3	-0.3	-0.2	-0.3	-0.7*	-0.6*

1024
 1025
 1026
 1027
 1028
 1029
 1030



1031

1032

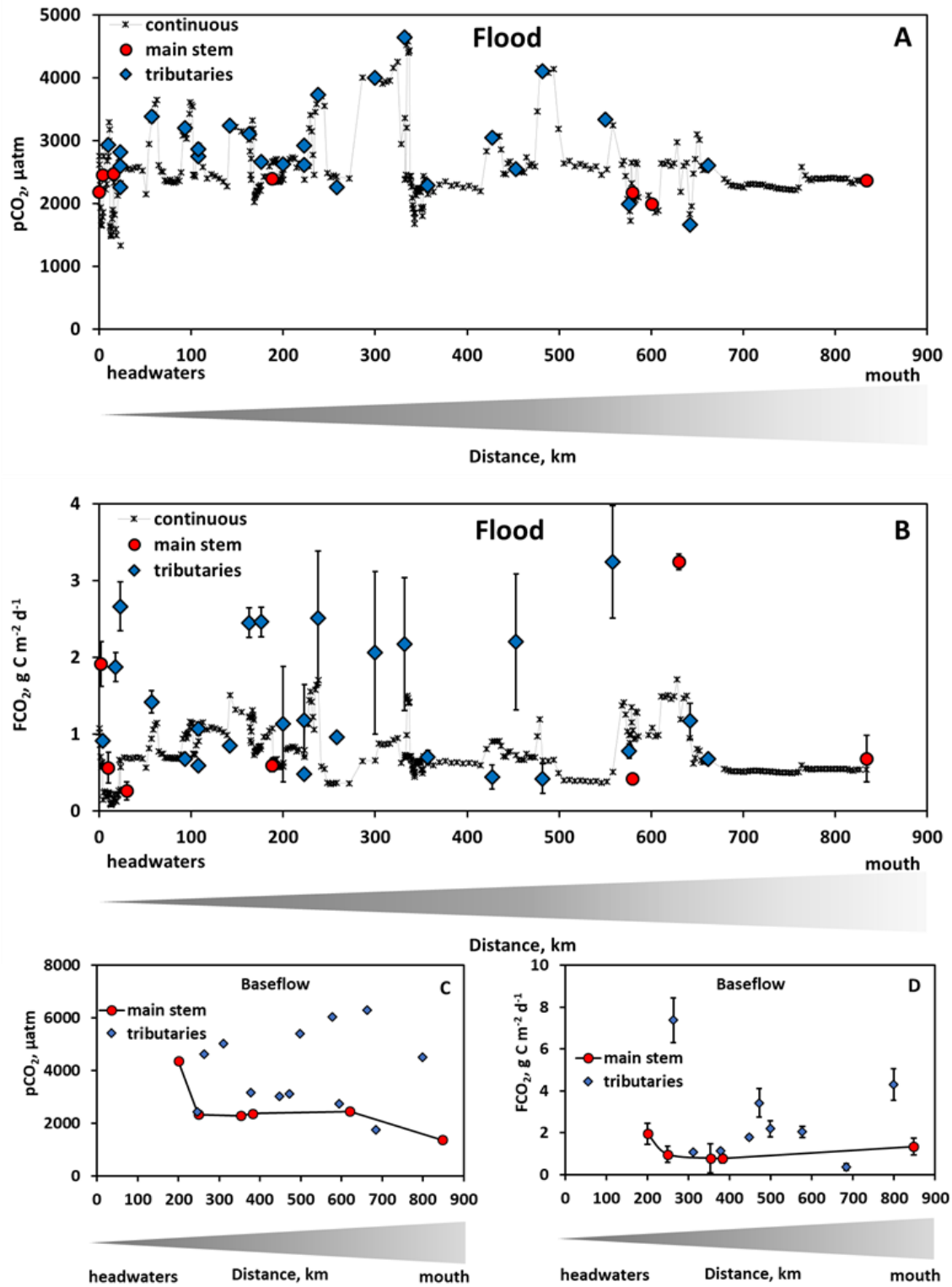
1033 **Fig. 1. A:** Map of the studied Ket River watershed with continuous pCO₂ measurements in the main stem.

1034 **B:** Daily discharge (Q) at the gauging station of the Ket mouth, Rodionovka, in 2019. Highlighted in blue

1035 and orange are two sampling campaigns of this study, spring flood and summer-autumn baseflow.

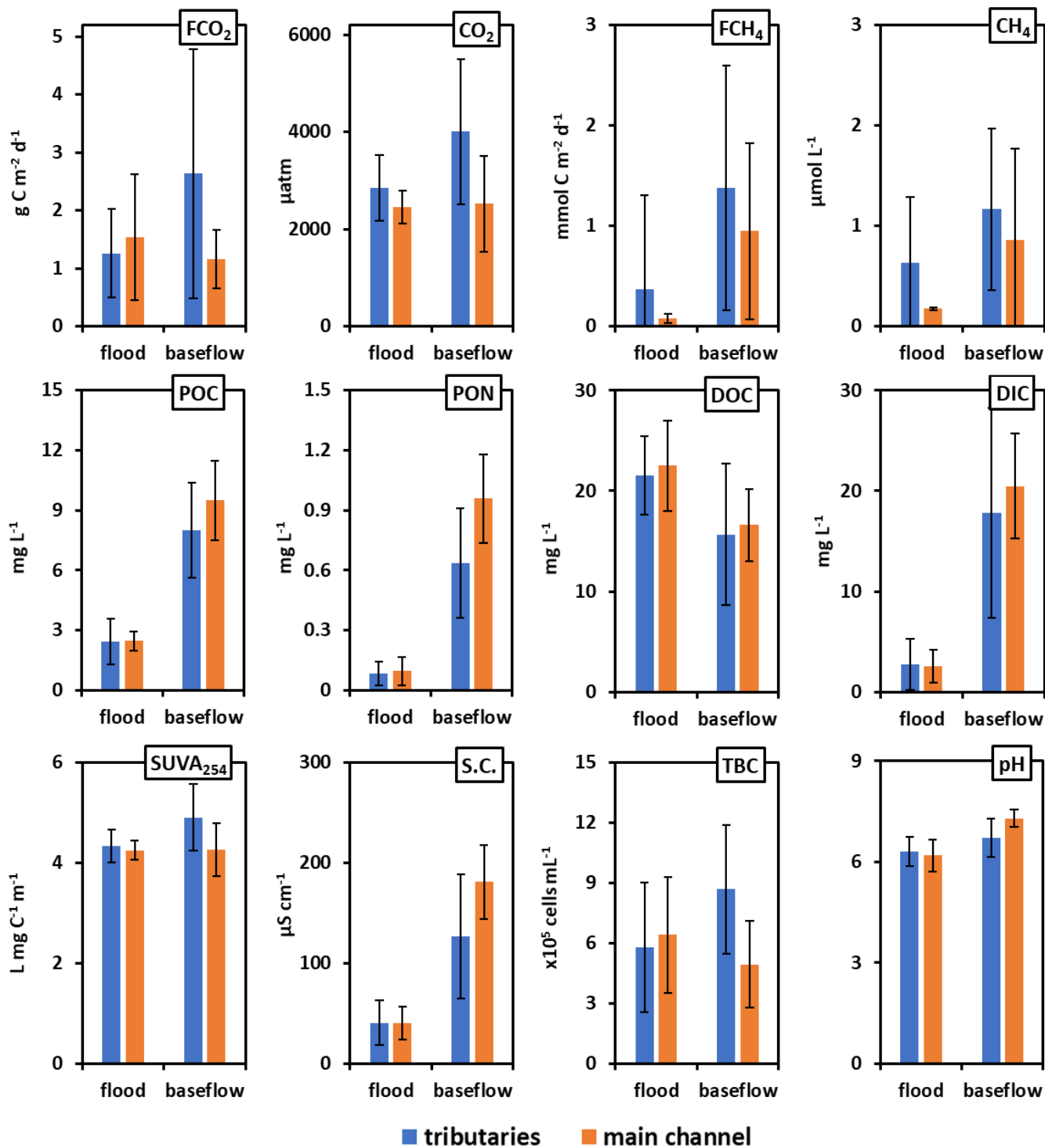
1036

1037



1038

1039 **Figure 2.** The measured pCO₂ (A, C) and CO₂ fluxes (B, D) during spring flood (A, B) and summer
 1040 baseflow (C, D) of the Ket River main stem and tributaries (over the 830 km distance, from the headwaters to
 1041 the mouth (left to right)). The symbols represent discrete in situ pCO₂ (Vaissala) and FCO₂ (floating
 1042 chambers) measurements of the main stem (red circles) and tributaries (blue diamonds). Continuous in-situ
 1043 pCO₂ measurements and calculated FCO₂ are available only for the main stem in spring (black crosses). For
 1044 the latter, we used an average value of gas transfer velocity (k_T) between two chamber sites (separated by a
 1045 distance of 50 to 100 km) to calculate the FCO₂ from in-situ measured pCO₂ in the river section between
 1046 these two sites. Note that during summer baseflow, the water level did not allow reaching the headwaters of
 1047 the Ket River (first 0-200 km on the river course).



1048

1049

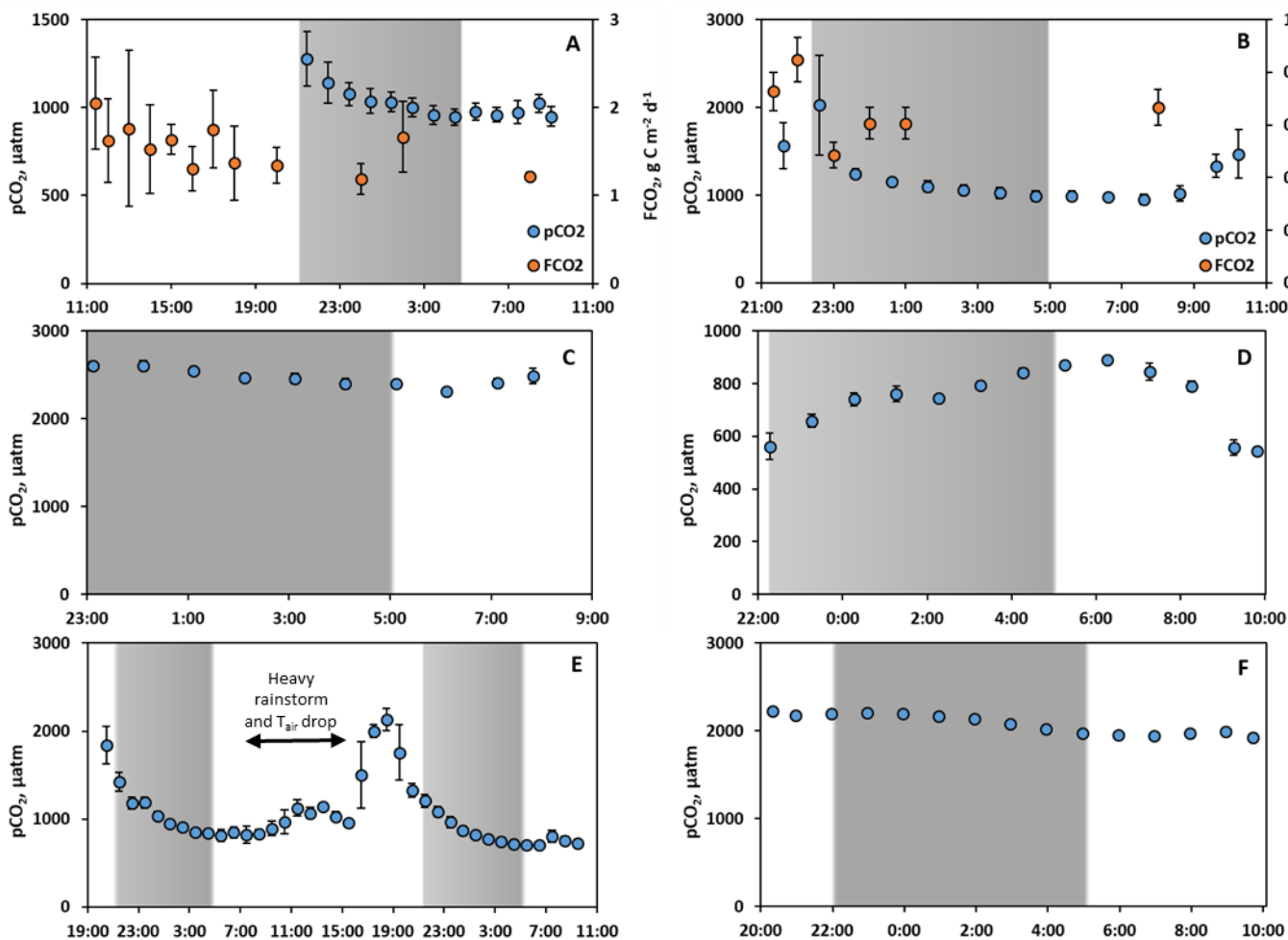
1050

1051 **Figure 3.** Mean (\pm s.d.) GHG concentration and fluxes, hydrochemical parameters, particulate organic
 1052 carbon and nitrogen (POC and PON, respectively) and total bacteria count (TBC), in the main channel
 1053 (orange column) and the tributaries (blue column) of the Ket River in spring flood and summer (early fall)
 1054 baseflow.

1055

1056

1057



1059

1060

1061

1062

1063

Figure 4. Continuous pCO₂ concentration (A-F, blue circles) and chamber-based fluxes (A, B) measured during spring flood period in tributaries (A Sochur No 3, B Lopatka No 8, C Derevyannaya No 12, D Ob river entrance, E Segondenka No 26) and in the Ket River main stem (middle course) near Stepanovka village (F) including night time measurements (shaded area). The measurement frequency was one per hour. Variations of water temperature were within the range of 0.3 to 0.6 °C and did not exhibit significant correlations with pCO₂ and FCO₂. Note that, for the small river Segondenka ($S_{\text{watershed}} = 472 \text{ km}^2$), where the CO₂ peak was observed at 7 pm (E), there was quite heavy rainfall between 7 am and 3 pm.

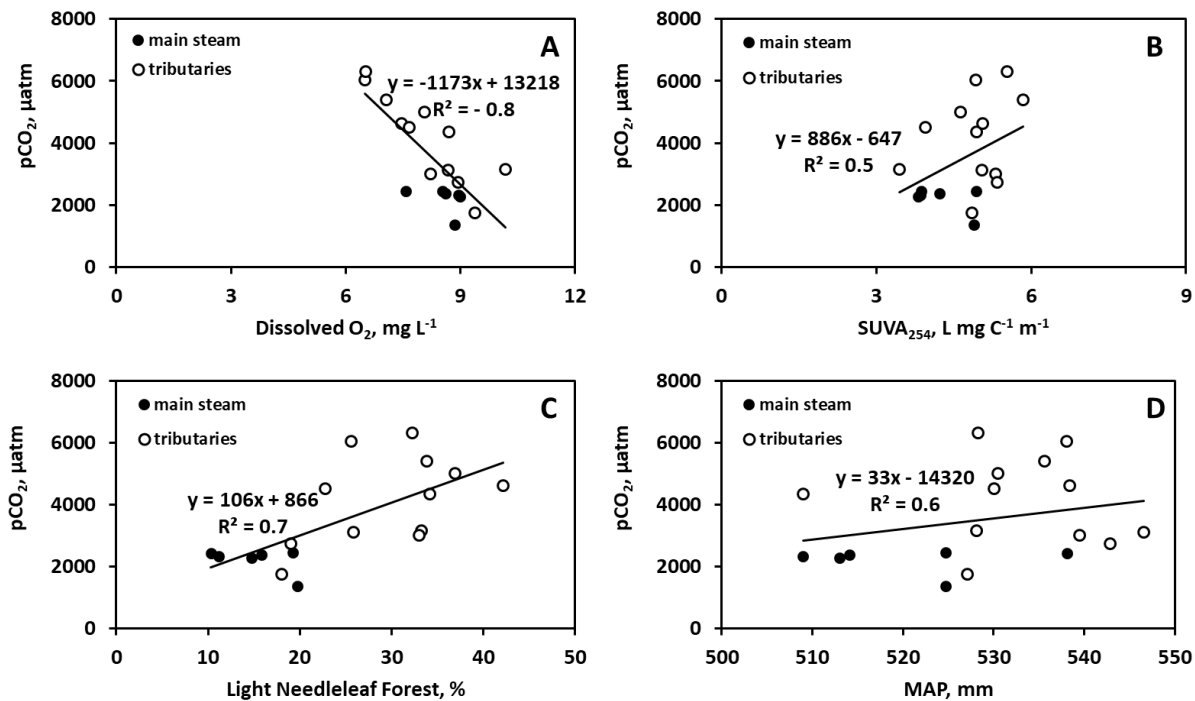
1071

1072

1073

1074

1075
1076
1077
1078
1079



1080
1081
1082
1083
1084
1085
1086
1087
1088
1089
1090
1091
1092
1093

Figure 5. Significant ($p < 0.05$) control of dissolved oxygen (A), SUVA₂₅₄ (B), light needleleaf forest (C), and mean annual precipitation (D) on CO₂ concentration in the Ket River and tributaries during summer baseflow.